Hindawi
Shock and Vibration
Volume 2018, Article ID 1917629, 26 pages
https://doi.org/10.1155/2018/1917629

Research Article

Deterministic and Probabilistic Serviceability Assessment of Footbridge Vibrations due to a Single Walker Crossing

Cristoforo Demartino,[1] Alberto Maria Avossa,[2] and Francesco Ricciardelli[2]

[1] *College of Civil Engineering, Nanjing Tech University, Nanjing 211816, China*
[2] *DICDEA, Università della Campania Luigi Vanvitelli, Via Roma 9, 81031 Aversa, Italy*

Correspondence should be addressed to Alberto Maria Avossa; albertomaria.avossa@unicampania.it

Received 9 July 2017; Revised 5 September 2017; Accepted 12 November 2017; Published 17 January 2018

Academic Editor: Hugo Rodrigues

This paper presents a numerical study on the deterministic and probabilistic serviceability assessment of footbridge vibrations due to a single walker crossing. The dynamic response of the footbridge is analyzed by means of modal analysis, considering only the first lateral and vertical modes. Single span footbridges with uniform mass distribution are considered, with different values of the span length, natural frequencies, mass, and structural damping and with different support conditions. The load induced by a single walker crossing the footbridge is modeled as a moving sinusoidal force either in the lateral or in the vertical direction. The variability of the characteristics of the load induced by walkers is modeled using probability distributions taken from the literature defining a Standard Population of walkers. Deterministic and probabilistic approaches were adopted to assess the peak response. Based on the results of the simulations, deterministic and probabilistic vibration serviceability assessment methods are proposed, not requiring numerical analyses. Finally, an example of the application of the proposed method to a truss steel footbridge is presented. The results highlight the advantages of the probabilistic procedure in terms of reliability quantification.

1. Introduction

Vibrations of footbridges due to human loading have recently received much attention, due to the increasing number of vibrations incidents occurring worldwide. The main cause of these large vibrations is the low stiffness and damping of recently built footbridges. As a matter of fact, if only static dead and live loads are considered in the design process, footbridges can prove unable to meet serviceability requirements against vibrations.

In particular, the significant amount of research produced in the last one and a half decades has been triggered by the two vibration incidents of the Paris Passerelle Solferino on December 15, 1999, and of the London Millennium Bridge on July 10, 2000, that played a similar role in the public opinion and in the scientific community to that played by the collapse of the Tacoma Narrows bridge in November 1940 [1]. Nevertheless, crowd-related failures of bridges have occurred over the centuries with much more devastating effects, the first of which being documented is probably that of the bridge over river Ouse in England, in 1154 [2]. In spite of the long series of failures, to the authors' knowledge the first paper to have appeared dealing with the effects of human movements on structural loading is that of Tilden [3]. This is a pioneering work where many aspects of the human loading of structures seem to have already been recognized, though not quantified.

The vibrations are generated by the "quasi" harmonic load induced by walkers and joggers. If the central frequency of the load and a natural vibration frequency of the footbridge are similar, resonant vibrations can occur. The latter is a rather common condition [4]. However, this apparently simple mechanism is in fact not easy to quantify. First of all, walkers do not induce a perfectly periodic load due to the intrasubject variability gait, and this load differs from one subject to another (intersubject variability). Finally, two forms of feedback can take place: (i) interwalker interaction and (ii) walker-structure interaction [5]. The first refers to gait modifications due to the presence of neighboring walkers, whereas the second is the adjustment of gait as an effect of the floor vibration.

Standards and guidelines have been developed to help the designer in the evaluation of the vibration serviceability based on simplified loading models, simulating different possible scenarios [5, 6]. In broad terms, the design of footbridges against pedestrian-induced vibrations requires the knowledge of [7] (i) the characteristics of the pedestrian action, (ii) a response evaluation method, and (iii) a comfort criterion. The interested reader is referred to [5, 6, 8, 9]. Design guidelines outline procedures for vibration serviceability checks, but it is noticeable that most of these assume that the action is deterministic [10], yet this is stochastic, and it would be reasonable to incorporate its variability in the loading models. However, it should be mentioned that other loads on bridges should be considered in the design procedures such as seismic, wind, and impact loads (e.g., [11–16]).

Different authors have tried to characterize the randomness of the pedestrian action in either time or frequency domain, considering both intrasubject and intersubject variability. Brownjohn et al. [17] for the vertical direction and Pizzimenti and Ricciardelli [18] and Ricciardelli and Pizzimenti [19] for the lateral direction gave Power Spectral Density Functions (PSDFs) of the load induced by a walker, for use in the evaluation of the stationary response to a stream of walkers, including intrasubject and intersubject variability of gait.

Subsequently, Butz [20] presented a spectral approach for the evaluation of the peak acceleration induced by unrestricted pedestrian traffic. The PSDFs of the modal force were approximated through a Gaussian function, fitting data coming from Monte Carlo simulations. These were carried out for different bridge geometries and for four different pedestrian densities. Step frequency, pedestrian mass, force amplitude, and pedestrian arrival time were randomly selected from given probability distributions. The PSDF of the acceleration was evaluated from the PSDF of the modal force, and the 95th fractile peak modal acceleration was derived as the product of the RMS acceleration and a peak factor. The latter was evaluated to be around 4. All the coefficients required for the application of the procedure were expressed in a parametric form. This model has then been incorporated into HIVOSS guidelines [21].

Živanović et al. [22] presented a multiharmonic force model for calculation of the multimode structural response to a crossing, accounting for inter- and intrasubject variability in the walking force. The model is again based on Monte Carlo simulations, with pedestrian characteristics also selected from given distributions. The intrasubject variability was accounted for describing the force in the frequency domain and then converting it to the time domain. No parametric form of the peak response as a function of the different parameters and no procedure for the serviceability assessment are given.

Ingólfsson et al. [23] proposed a Response Spectrum approach inspired by earthquake engineering. Through Monte Carlo simulations, they evaluated a reference vertical acceleration to the action of a flow of 1 walker/s with probabilistically modeled characteristics, to which empirical correction factors are applied to account for return period, modal mass, mean arrival rate, structural damping, footbridge span, and mode shape. A total of 97 windows, 300 s long, were used to establish the peak acceleration Generalized Extreme Value (GEV) distribution parameters. Two reference populations were considered, with step frequencies of 1.8 and 2.0 Hz, with STD of 0.1 Hz and Poisson distributed arrivals. The input force was modeled as a harmonic load and the intersubject variability was considered varying the characteristics of each pedestrian according to given distributions. All the parameters contained in the procedure are given in parametric form, and the GEV distribution of the peak acceleration is found to tend to a Gumbel distribution (i.e., the shape parameter tends to 0).

Piccardo and Tubino [24] studied the vertical vibration serviceability of footbridges, based on a probabilistic characterization of pedestrian-induced forces taking into account intersubject variability and considering only one mode of vibration. Only the 95th fractile peak modal acceleration was derived and expressed in two nondimensional forms: (a) the Equivalent Amplification Factor, that is, the ratio between the maximum dynamic response to a realistic loading scenario and the maximum dynamic response to a single resonant pedestrian; (b) the Equivalent Synchronization Factor, that is, the ratio between the maximum dynamic response to a realistic loading scenario and the maximum dynamic response to uniformly distributed resonant pedestrians. Comparison of their procedure with similar methods contained in standards and design guidelines has pointed out that the latter are generally conservative (often largely conservative) and can become only slightly nonconservative in particular cases. They concluded that further investigations on the evaluation of the PDF of the maximum dynamic response are required.

Živanović et al. [25] reviewed different time-domain design procedures for vibration serviceability assessment of footbridges exposed to streams of pedestrians and evaluated their performance in predicting the vertical vibration response of two existing footbridges. They compared the procedures contained in Eurocode 5 [26], ISO 10137 [27], Sétra [28], BSI [29], Brownjohn et al. [30], Butz [20], Ingólfsson et al. [23], and Živanović et al. [22]. They found some discrepancies between the predicted and measured vibration levels and discussed their potential causes, among which are interwalker and walker-structure interaction.

Pedersen and Frier [10] evaluated the effect of the probabilistic modeling of the parameters describing walking loads: step frequency, stride length, Dynamic Load Factor (DLF), and walker weight. A literature review revealed a variety of probability distributions through which the walking parameters can be modeled, and these were used for exploring the sensitivity of the 95th fractile of midspan acceleration. They observed that the step frequency distribution can have a strong influence, whereas the DLF, the walker weight, and stride length have a much lower influence. No interactions were considered in this study.

Ingólfsson and Georgakis [31] presented a probabilistic lateral load model in which the forces are given as the sum of an external component and a frequency and amplitude-dependent self-excited component; the latter is quantified through equivalent pedestrian damping and mass coefficients measured from experiments. They found that the peak

response of a footbridge to a pedestrian flow is very sensitive to the selection of the pacing rate distribution.

Piccardo and Tubino [32] introduced an equivalent spectral model for the analysis of the dynamic response of footbridges to unrestricted pedestrian traffic (i.e., no interwalker interaction) using a complete probabilistic representation of pedestrians. They provided simple closed-form expressions for the evaluation of the maximum dynamic response for use in vibration serviceability analyses, similarly to classical procedures adopted in wind engineering. These expressions are based on the definition of the peak factor found by Davenport [33].

Recently, Ricciardelli and Demartino [5] compared background hypotheses, fields of applicability, and results obtained through a number of different loading and response evaluation models. In particular, they compared single walker models, multiple walkers models, interaction models (interwalker and walker-structure), and instability models, together with current design procedures incorporated into standards and guidelines. Avossa et al. [34] applied the design procedures to various steel footbridges highlighting the large differences that they bring in the results. They concluded that a critical revision of design procedures is needed as these, even though inspired by the same principles and applying the same rules, show different results; this should also be done through validation with the available full-scale data. Finally, Avossa et al. [35] evaluated through Monte Carlo simulations the probability distribution of the footbridge peak acceleration to single and multiple crossing walkers for two specific footbridge configurations.

In combination with a probabilistic definition of the load, criteria for the probabilistic definition of the structural capacity must be set. For instance, Eurocode 0 [36] requires that a structure is designed to have adequate (i) resistance, (ii) serviceability, and (iii) durability. In particular, the limit state of vibrations causing discomfort to people and/or limiting the functional effectiveness of the structure must be considered. Moreover, it establishes that when the structure is prone to significant acceleration, dynamic analyses must be performed. Similarly, ISO 2394 [37] specifies general principles for the reliability assessment of structures subjected to known or foreseeable types of actions, providing more or less similar requirements for safety, serviceability, and durability. In Annex E of ISO 2394 [37], principles of reliability-based design are given specifying the requirements in terms of probability of failure for different limit states.

ISO 10137 [27] contains structural acceleration limits for different situations. ISO 10137 recognizes the vibration source, path, and receiver as three key elements which require being identified when dealing with vibration serviceability. In the context of walking-induced vibrations in footbridges, the walkers are the vibration source, the footbridge is the path, and the walkers are again the receivers. According to ISO 10137, an analysis of the response requires a calculation model that incorporates the characteristics of the source and of the transmission path, which must be solved for the vibration response of the receiver; in doing so, the dynamic action of one or more walkers can be described as force time histories. This action varies in time and space as the walkers move on the footbridge. It is recommended that the following scenarios are considered: (i) one person walking across the bridge, (ii) an average pedestrian flow (group size of 8 to 15 walkers), (iii) streams of walkers (significantly more than 15 walkers), and (iv) occasional festive choreographic events (when relevant).

However, although many authors have derived probabilistic models to describe the vibration response induced by pedestrian loads, a fully probabilistic procedure for the serviceability assessment of footbridge vibrations due to a single walker crossing and a comparison with deterministic approaches is not yet available. In particular, the studies reviewed above do not allow for variation of the reliability levels, as they take as demand parameter the 95th fractile of the peak acceleration response. It is important to notice that although the research interest is nowadays mainly oriented towards the multipedestrian case, the need for analyzing the single pedestrian case stems from at least three different reasons: (i) this case can induce the largest acceleration, especially for short low-damped footbridges, (ii) many standards and codes of practices refer to this load scenario, and (iii) vibration assessment procedures for multipedestrian loading are often derived from the single pedestrian case.

This study presents criteria for the deterministic and probabilistic vibration serviceability assessment of footbridges to the crossing of one walker. In Section 2, the load induced by a single walker is modeled as a moving harmonic force having lateral and vertical components, whose characteristics derive from a Standard Population (SP) of walkers. The latter is defined based on data available in the literature, concerning the probabilistic distribution of walker characteristics and gait parameters. In Section 3, the dynamic characteristics of a single span footbridge (span length, natural frequencies, mass, structural damping, and support conditions) are defined and a modal dynamic model is presented. In Section 4, numerical analyses of the transient response to a moving harmonic load are presented, through which the peak response is evaluated in both a deterministic and probabilistic way. In Section 5, closed-form deterministic and probabilistic vibration serviceability methods are proposed, whose applications do not require numerical analyses. These incorporate the acceleration limits of ISO 10137 [27] and the required reliability level of ISO 2394 [37], leading to a method which also complies with Eurocode 0 [36]. As an example, in Section 6, the deterministic and probabilistic methods are applied to a prototype truss steel footbridge. Finally, some conclusions and prospects are drawn (Section 7).

2. Single Walker Behavior

Ground Reaction Forces (GRFs) are defined as the forces induced on the ground by walkers. The measurement of GRFs has advanced considerably over the recent decades. It first became a useful clinical tool starting from the pioneering work of Beely [38] and Elftman [39]. Nowadays, observational gait analysis is regularly performed by physical therapists to determine treatment goals and is used as an evaluation tool during rehabilitation [40]. In Medical Sciences, the main goal is the identification of the kinematic characteristics

of a subject. Differently, in civil engineering it is of interest to characterize GRFs, with the final aim of evaluating the structural response for comfort assessment [9, 41].

GRFs are characterized by different magnitudes and frequency content in the vertical, lateral, and longitudinal directions. Based on the existing knowledge of GRFs, several loading models have been developed for footbridges, some of which consider the crossing of a single pedestrian [5]. A common approach is that of periodic loading, assuming that a walker generates identical footfalls with constant frequency neglecting intrasubject variability. In this case, the dynamic part of the GRF is expanded in Fourier series:

$$F_i(t) = W \cdot \sum_{j=1}^{\infty} \mathrm{DLF}_{i,j} \left(\sin\left(j \cdot \pi \cdot f_{w,i} \cdot t\right) - \psi_{i,j}\right), \quad (1)$$

where the subscript $i = V, L$ indicates the vertical or lateral direction (the longitudinal component is neglected) and where W is the weight of the walker, $\mathrm{DLF}_{i,j}$ is the jth Dynamic Load Factor (DLF), that is, the jth harmonic load amplitude normalized by the body weight, $f_{w,i} = f_w$ when $i = V$ and $f_{w,i} = 0.5 \cdot f_w$ when $i = L$, f_w being the step frequency, and $\psi_{i,j}$ is the phase lag of the jth harmonic. Moreover, in the following, only the first harmonic will be retained, and accordingly subscript j will be omitted. This representation of the load is consistent with different standards such as UK Annex to EC1 [29] and ISO 10137 [27].

When the walker crosses a footbridge of span L, the modal load associated with the first bending mode is

$$f_i(t) = \int_0^L \phi_i(x) \cdot F_i(t) \cdot \delta(x - v \cdot t) \cdot \left[H(t) - H\left(t - T_p\right)\right] \mathrm{d}x, \quad (2)$$

where $\phi_i(x)$ is first mode shape (Section 3), $\delta(\bullet)$ is the Dirac Function, x defines the position of the walker on the bridge, $H(\bullet)$ is the Heaviside function, and $T_p = L/v$ is the crossing time, $v = f_w l_w$ being the walking speed, L the span length, and l_w the step length.

2.1. Standard Population of Walkers. The definition of a Standard Population (SP) of walkers is needed to characterize intersubject variability probabilistically. This is not trivial due to the large scatter of the data available in the literature, and one must be aware of the fact that changing the population will lead to a different vibration response [10].

The parameters governing the excitation generated by a walker are (i) the walking speed v, (ii) the step frequency f_w, (iii) the Dynamic Load Factors DLF_V and DLF_L, (iv) the weight of the walker W, and (v) the phase angles ψ_V and ψ_L. The data mainly come from the Biomechanics and Transportation fields, although recent results have also been published in the area of structural engineering. The SP defined in this section is based on research developed in European countries.

Humans can walk up to 4 m/s [42], but the speed of roughly 2.2 m/s represents a natural transition from walking to running [43, 44]. In spite of this, the walking speed is usually considered as normally distributed, and a large scatter in the mean value is found in the literature. This is due to physiological and psychological factors, such as biometric characteristics of the walker (body weight, height, age, and gender), cultural and racial differences, travel purpose, and type of walking facility [45]. In the following, the walker speed is assumed as [46]

$$v = \mathcal{N}(1.41, 0.224) > 0.41 \ [\mathrm{m/s}]. \quad (3)$$

Equation (3) is truncated at 0.41 m/s as smaller values lead to negative STDs in (4).

It is agreed that walking occurs at an average step frequency of approximately $f_w = 2$ Hz (e.g., [28]). Biomechanics studies established that walkers tend to adjust their step frequency and therefore step length, l_w, so to minimize energy consumption at a given walking speed [47]. The step length (and its double, the stride length) varies with the physical characteristics of the subject (height, weight, etc.) and from one country to another due to the different traditions and lifestyle. Accordingly, the correlation between the walking speed and the step frequency has been reported in literature with a large scatter [45, 48–50]. Many researchers have considered the step frequency as normally distributed [41, 48, 51]. In this study, it is assumed that the mean and STD of the normal distribution of f_w are linearly dependent on the walking speed [52]:

$$f_w = \mathcal{N}(0.7868 \cdot v + 0.7886, 0.0857 \cdot v - 0.035) > 0 \ [\mathrm{Hz}]. \quad (4)$$

Negative values are truncated as meaningless. The mean value of f_w associated with the mean walking speed (i.e., 1.41 m/s) is 1.898 Hz, and the standard deviation is 0.086 Hz.

Values of the DLFs have been reported in many publications and have been incorporated into design guidelines. These are usually derived from force measurements on instrumented floors or treadmills [53]. In this study, only fixed floor conditions are considered since walker-structure interaction effects are neglected. This interaction is significant in the lateral direction [54] and less in the vertical direction. DLFs measured on a rigid floor are therefore assumed to be the same as those that would be measured on a moving floor if the displacements are small. Moreover, DLFs can also be derived using analytical models that are usually inspired by biomechanics as the inverted pendulum model [55, 56]. Živanović et al. [8] reported a review of the DLFs used in single walker force models. The mean values of DLF_V are approximately in the range of 0.257 [57] to 0.5 [58]. Generally, the dynamic part of the vertical GRF is found to be dependent on f_w. The first study revealing this issue is that of Kajikawa [59] (reported in [60]). It is now widely accepted that DLF_V increases with f_w up to a maximum of approximately 0.5 [61, 62]. Accordingly, in this study, the SP is described through a DLF_V depending on f_w (see (4)) as [62]

$$0 < \mathrm{DLF}_V = 0.37 \cdot \left(f_w - 0.95\right) \leq 0.5. \quad (5)$$

According to (5), DLF_V is described by a normal distribution with mean equal to 0.35 and STD 0.07.

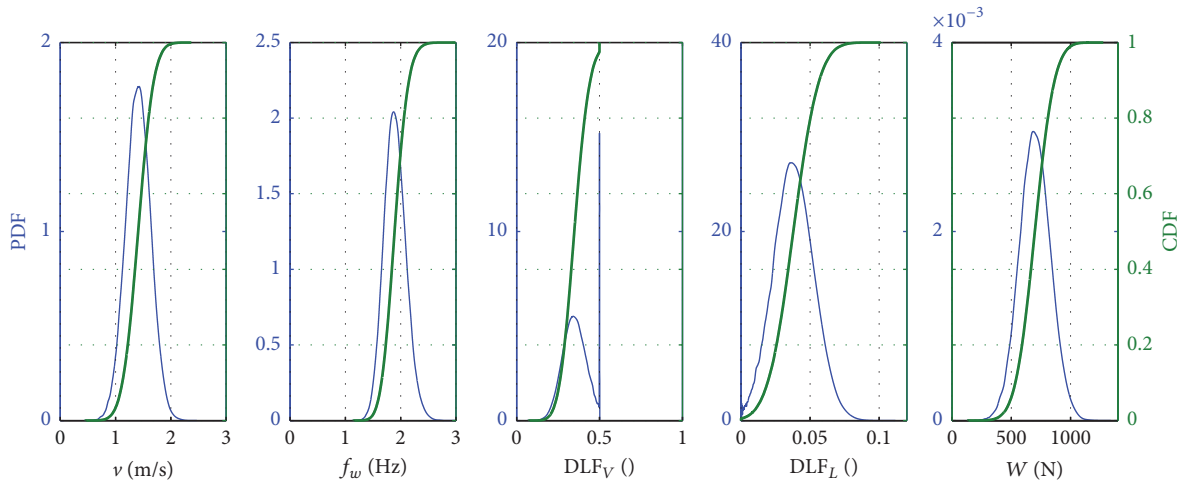

Figure 1: Probability Density Function (PDF, thin line) and Cumulated Distribution Function (CDF, thick line) of the random variables defining the SP: v, f_w, DLF$_V$, DLF$_L$, and W.

On the other hand, the mean values of DLF$_L$ are approximately in the range of 0.039 [63] to 0.1 [58]. Accordingly, in this study, the SP is assumed to have a DLF$_L$ described through a normal distribution [52]:

$$\mathrm{DLF}_L = \mathcal{N}(0.03792, 0.01459) > 0. \tag{6}$$

In (5) and (6), negative values are truncated as meaningless. Moreover, in (5) an upper bound was set at 0.5.

The body weight is very much dependent on height; therefore, in medical applications, it is preferred to refer to the Body Mass Index (BMI), that is, the body mass divided by the square of the height [64]. For each country, Walpole et al. [65] used available data on BMI and height distribution to estimate average adult body mass. In particular, they reported the average body mass by world regions as in 2005. The average body mass ranges between 57.7 kg for Asia and 80.7 kg for North America. Indeed, load models (e.g., (1)) require the definition of the walker weight, W; that is, the body weight increased by the weight of clothing and other items carried by the walker. The walker weight is taken equal to 700 N by many loading models (e.g., [28, 57]). In this study, the weight of the SP is assumed to be normally distributed as in HIVOSS [21]:

$$W = \mathcal{N}(744, 130) \geq 0 \ [\mathrm{N}]. \tag{7}$$

The mean value in (7) is 7% larger than that of 695 N corresponding to the average body mass 70.8 kg reported by Walpole et al. [65] for Europe since the latter lacks clothing and other items carried by the walker. Negative values are truncated as meaningless.

Finally, the distribution of phase lags, ψ_i, between walkers is a measure of the correlation of the forces they exert. For a continuous PDF of walking frequencies, phase lags are characterized by the PDF of the phase spectrum. If this is uniformly distributed between 0 and 2π, then the walkers and the walking forces are uncorrelated. Correlation increases when the PDF of the phase spectrum is peaky around a given value as this value approaches 0; the forces tend to be in phase. In the case of a single walker, all this loses its meaning and will be neglected in the following.

In Figure 1, the Probability Density Functions (PDFs) and the Cumulative Distribution Functions (CDFs) of the random variables defining the SP previously described are shown.

3. Footbridge Characteristics and Mechanical Model

In this study, single span beam footbridges are considered. The dynamic response of the footbridge is analyzed by means of modal analysis, considering only the first lateral and vertical modes. The latter assumption is made since (i) in common footbridges torsional vibrations are not an issue, with the exception of some research aimed at the mitigation of torsional vibrations on suspended footbridges [66] and (ii) usually only one mode, either vertical or lateral, is responsible for the footbridge liveliness [67].

Referring to Figure 2, the footbridge response is governed by the two uncoupled differential equations ($i = V, L$):

$$\begin{aligned} m\ddot{u}_i(x,t) + c_i\dot{u}_i(x,t) + EI_i u_i^{IV}(x,t) \\ = F_i(t) \cdot \delta(x - v \cdot t), \end{aligned} \tag{8}$$

where m is the footbridge uniform mass per unit length, c_i is the viscous damping per unit length and EI_i is the bending stiffness, and $u_i(x,t)$ are the displacements in the vertical, $u_V(x,t)$, and lateral, $u_L(x,t)$, directions. $F_i(t)$ and $\delta(x - v \cdot t)$ have been defined in Section 2. The viscous damping is related to the inherent structural damping and to that based on isolation or supplemental energy dissipation devices (e.g., [68, 69]).

Considering only one mode of vibration, the vertical and lateral deflection of the footbridge is written as

$$u_i(x,t) = \phi_i(x)\eta_i(t), \tag{9}$$

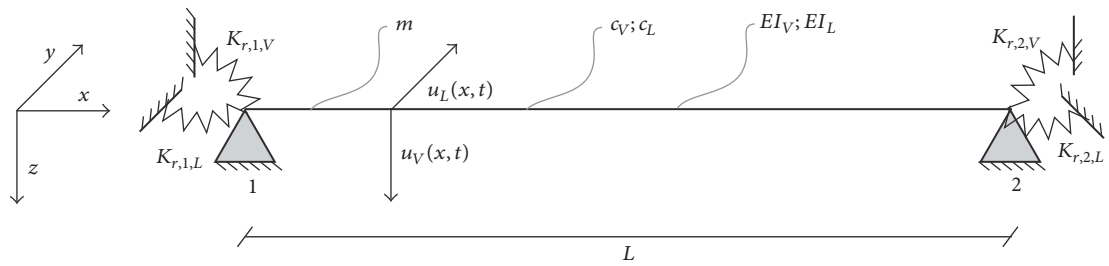

Figure 2: Beam characteristics: dynamic model.

where $\phi_i(x)$ is the mode shape and $\eta_i(t)$ the associated generalized coordinates in the vertical, $\eta_V(t)$, and lateral, $\eta_L(t)$, directions.

For a single span beam, the mode shape takes the general form:

$$\phi_i(x) = c_{1i}\sin\left(\lambda_i\frac{x}{L}\right) + c_{2i}\cos\left(\lambda_i\frac{x}{L}\right) + c_{3i}\sinh\left(\lambda_i\frac{x}{L}\right) + c_{4i}\cosh\left(\lambda_i\frac{x}{L}\right), \tag{10}$$

where λ_i is the first eigenvalue of the secular equation and c_{1i}, c_{2i}, c_{3i}, and c_{4i} depend on the supports rotational stiffness $K_{r,1,i}$ and $K_{r,2,i}$ (Figure 2). For example, for a simply supported beam ($K_{r,1,i} = K_{r,2,i} = 0$), $c_{1i} = 1$ and $c_{2i} = c_{3i} = c_{4i} = 0$ and $\lambda_i = \pi$. The mode shape is normalized, so as to have maximum value equal to one.

The modal equations of motion are

$$\ddot{\eta}_i(t) + 4\pi\xi_i f_i\dot{\eta}_i(t) + 4\pi^2 f_i^2\eta_i(t) = m_i^{-1} f_i(t), \tag{11}$$

where ξ_i is the modal damping ratio, f_i is the natural frequency, and m_i is the modal mass in the vertical and lateral directions.

Assuming that the motion starts from rest (i.e., $\eta_i(0) = \dot{\eta}_i(0) = 0$), the solution of (11) is

$$\eta_i(t) = \frac{1}{m_i}\int_o^t f_i(\tau)\cdot h_i(t-\tau)\cdot \mathrm{d}\tau, \tag{12}$$

where $h_i(t-\tau)$ is the unit-impulse response function.

The governing parameters of the dynamic response are (i) the span length L, (ii) the natural frequencies f_V and f_L, (iii) the structural damping ratios ξ_V and ξ_L, and (iv) the modal shapes $\phi_V(x)$ and $\phi_L(x)$. The footbridge mass per unit length, m, also influences the response. However, this parameter appears as a linear factor in the equations and accordingly it plays the role of a scale parameter in the results.

In the analyses, values of the span length L in the wide range of 10 m to 200 m were considered, where the smallest value corresponds to a simple road crossing and the largest is assumed as an upper limit for beam footbridges.

The vertical and lateral natural frequencies are expressed in terms of frequency ratios: $\alpha_i = \overline{f}_{w,i}/f_i$. Here and in the following, the overbar indicates a mean value of the distribution. The range of interests for vibration serviceability assessments is $0.3 \le \alpha_i \le 1.7$, which approximately corresponds to the external boundaries of Range 3 (low risk of resonance for standard loading situations) as defined in Sétra [28].

The damping ratio can vary in the wide range of 0.1% to 2.0% [70]. In particular, standards and guidelines, such as Sétra [28], Heinemeyer et al. [21], ISO 10137 [27], and Eurocodes (EC1 [71], EC3 [72], and EC5 [26]), suggest minimum and mean values depending on construction material (Table 1). The lower values apply to steel bridges (0.2% ÷ 0.5%), whereas the largest values are for timber bridges (1.5% ÷ 3%). In particular, the values given by FIB [73] are the result of the combination of material, bridge type, and support conditions. According to the values given in Table 1, damping ratios in the range of 0.1% to 1.5% were considered in this study. It is worth mentioning that it is difficult to accurately predict (during the design process) and estimate (during the assessment process) this parameter and accordingly fairly large uncertainties are associated with it.

Finally, the mode shapes (i.e., the supports rotational stiffness values $K_{r,1,i}$ and $K_{r,2,i}$) influence the dynamic response of the footbridge. In particular, the mode shapes vary the modal masses, m_V or m_L, and the modal loads (see (2)). Mode shapes (see (10)), in turn, depend on the rotational stiffness of the supports, $K_{r,1,i}$ and $K_{r,2,i}$. In this study, only symmetric support conditions have been considered, that is, $K_{r,1,i} = K_{r,2,i} = K_{r,i}$.

In general, the mode shapes are a function of $K_{r,i}$. However, when the mode shape is evaluated from a FE model, the evaluation of the end rotational stiffness can be cumbersome and also a direct comparison to fit (10) is not immediate. Accordingly, in the following, a simplified and approximate procedure is proposed to define the mode shapes of the equivalent beam model (i.e., (10)) using static analysis from the FE model of the footbridge. The only reason for this simplified procedure is to provide practitioners with a simple tool to apply the proposed method. This method is accurate if the FE model meets the assumptions of (10), that is, constant mass and stiffness. To this aim, the support condition is expressed in terms of a nondimensional restrained level (RL), defined as the ratio of the end moment for the particular support condition (i.e., value of $K_{r,i}$) due to an arbitrary symmetric load, $M_i(K_r)$, to that of the clamped beam subjected to the same load, $M_i(K_r \to \infty)$:

$$\mathrm{RL}_i = \frac{M_i(K_{r,i})}{M_i(K_{r,i} \to \infty)}. \tag{13}$$

Table 1: Suggested damping ratios ξ [%] for different construction material, as given by different standards and guidelines.

Type	Damping ratios ξ [%]							
	Sétra		Hivoss		ISO 10137	Eurocodes[1]	FIB	
	Min	Mean	Min	Mean	Mean	Mean	Min	Mean
Reinforced concrete	0.8	1.3	0.8	1.3	0.8	1.5	0.8	1.2
Prestressed concrete	0.5	1.0	0.5	1.0		1.0	0.7	1.0
Steel	0.2	0.4	0.2	0.4	0.5	0.2/0.4[2]	0.5	1.0
Composite steel-concrete	0.3	0.6	0.3	0.6	0.6	0.6	0.6	1.0
Timber	1.5	3.0	1.0	1.5	-	1/1.5[3]	0.8	1.4

[1]EC1 [71], EC3 [72], and EC5 [26]; [2]0.2/0.4% if welded/bolted connection are present; [3]1% if no mechanical joints are present and 1.5% otherwise.

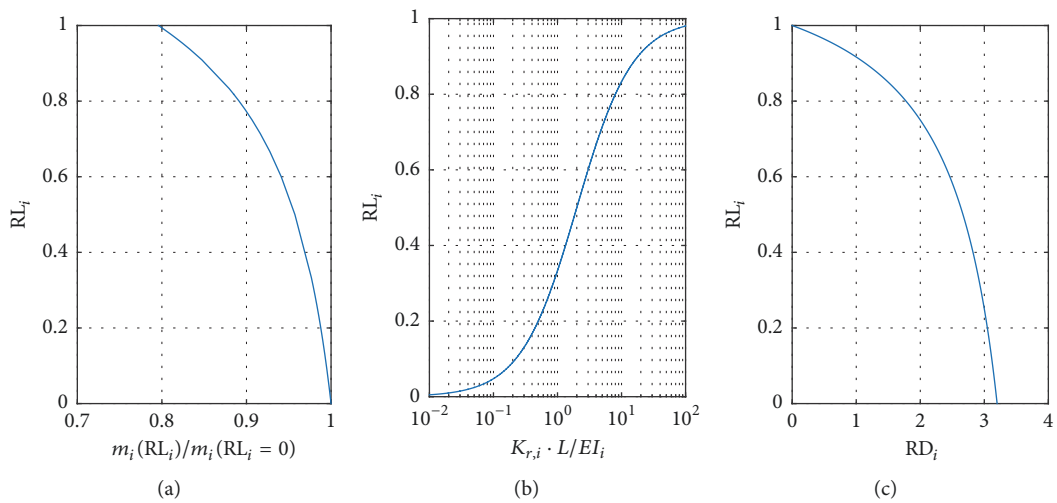

Figure 3: Restrained level RL_i as a function of $m_i(\mathrm{RL}_i)/m_i(\mathrm{RL}_i = 0)$ (a), $K_{r,i}L/EI_i$ (b), and RD_i (c).

Therefore, RL_i is in the range of 0 (supported case, $K_{r,i} = 0$) to 1 (clamped case, $K_{r,i} \to \infty$). The relationship between $K_{r,i}$ and RL_i can be simply obtained as

$$K_{r,i} = 2 \cdot \frac{\mathrm{RL}_i}{1 - \mathrm{RL}_i} \cdot \frac{EI_i}{L}. \tag{14}$$

The relationship between $K_{r,i}$ and RL_i is shown in a nondimensional form in Figure 3. The derivation of (14) is given in Appendix C.1.

On the other hand, the static deformation due to an arbitrary uniform load of the Finite Element model is expressed as the nondimensional Rotation-to-Deflection ratio (RD_i):

$$\mathrm{RD}_i = \frac{\Theta_i \cdot L}{\delta_i}, \tag{15}$$

where θ_i and δ_i are the end rotation and midspan deflection. The relationship between RL_i and RD_i can be simply obtained as

$$\mathrm{RL}_i = \frac{4 - 1.25 \cdot \mathrm{RD}_i}{4 - \mathrm{RD}_i} \tag{16}$$

which is also shown in Figure 3. Finally, the parameters of (10) are chosen in order to have the same value of RD_i as that obtained from the FE model. The derivation of (16) is given in Appendix C.2.

To conclude, the simplified and approximated procedure to evaluate the mode shape using static analysis of the FE model of the footbridge requires the following steps: (i) evaluation of RD_i (see (15)) using the FE model of the footbridge (i.e., evaluation of the end rotation and midspan deflection, θ_i and δ_i, due to a uniform load), (ii) conversion of RD_i to an equivalent RL_i using (16) (Figure 3), (iii) evaluation of $K_{r,i}$ using (14) (Figure 3), and (iv) evaluation of the mode shapes (see (10)) using as input the obtained $K_{r,i}$ in the boundary conditions and solving the eigenvalue problem obtaining λ_i, c_{1i}, c_{2i}, c_{3i}, and c_{4i}. Finally, by integrating the mass per unit length, m, over the mode shape, the modal mass can be obtained. The ratio of the modal mass for the generic boundary, $m_i(\mathrm{RL}_i)$, to the modal mass of the supported beam, $m_i(\mathrm{RL}_i = 0)$, is shown as a function of RL_i in Figure 3. This was obtained by numerically solving the eigenvalue problem for different values of RL_i. As expected, the modal mass reduces when the rotational stiffness of the supports increases (i.e., RL_i). The latter ratio will be used in Section 4.1.2.

4. Response Evaluation

In this section, the response evaluation procedure is presented. This is summarized in Figure 4. The aim of the assessment is to verify that the acceleration induced by the crossing of a single walker is not causing discomfort to the walker

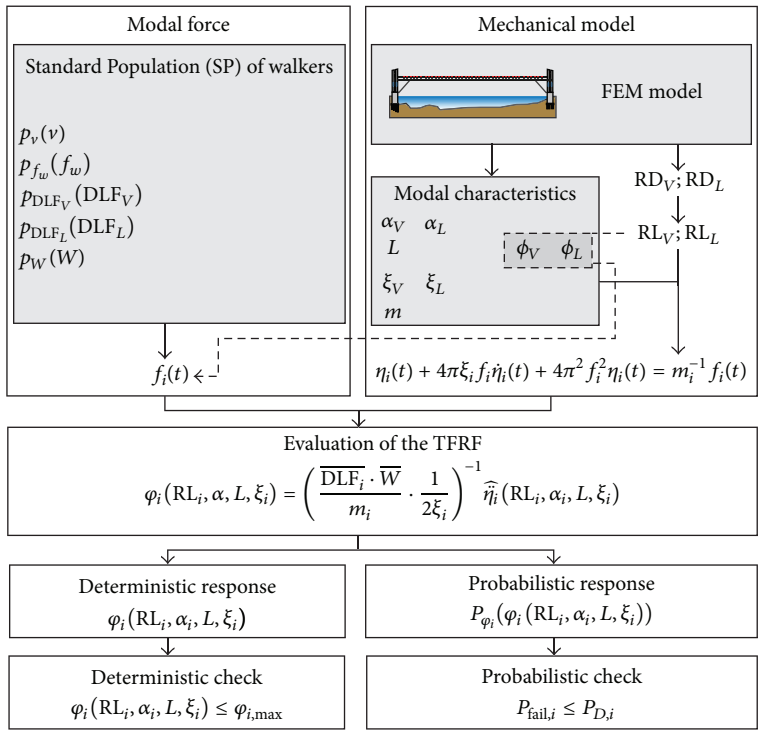

Figure 4: Deterministic and probabilistic assessment procedures.

himself/herself or other people standing on the footbridge. The engineering demand parameter chosen to assess this scenario is the peak acceleration, as it will be shown in Section 5. A deterministic and a probabilistic approach will be used.

The input parameters are characteristics of the walker (modal force) and the dynamic properties of the footbridge (mechanical model). The SP described in Section 2.1 is used to describe the characteristics of the walker and of the induced modal force. The deterministic response is evaluated referring to the SW (i.e., the walker having mean characteristics of the SP). The probabilistic response is evaluated referring to the SP defined in Section 2.

The output is expressed through the Transient Frequency Response Function (TFRF), that is, the ratio between the modal peak nonstationary response induced by a given walker crossing the bridge and the corresponding stationary response induced by the SW. In this way, the peak modal acceleration, $\widehat{\ddot{\eta}}_i$, can be expressed in terms of a TFRF [5, 75]:

$$\widehat{\ddot{\eta}}_i\left(\mathrm{RL}_i, \alpha_i, L, \xi_i\right) = \frac{\overline{\mathrm{DLF}_i} \cdot \overline{W}}{2\xi_i} \cdot \frac{1}{m_i} \cdot \varphi_i\left(\mathrm{RL}_i, \alpha_i, L, \xi_i\right), \quad (17)$$

where φ_i is the TFRF. Here and in the following, the hat, $\hat{\bullet}$, indicates the peak response and the overline, $\bar{\bullet}$, indicates the mean value. The mechanical model of the footbridge is deterministic and the response is expressed as a function of its input parameters:

$$\begin{aligned} \mathrm{RL}_i &\longrightarrow \text{mode shape,} \\ \alpha_i &\longrightarrow \text{frequency ratio,} \\ \xi_i &\longrightarrow \text{damping ratio,} \\ L &\longrightarrow \text{number of loading cycles.} \end{aligned} \quad (18)$$

The arrow indicates to which characteristics of the mechanical model or modal force the input parameters are referred. In particular, the first three are nondimensional parameters, defining the dynamic properties of the structure. The last is the dimensional footbridge span, which is a measure of the number of loading cycles (see (2)). The number of cycles is the ratio of L to the wavelength, the latter being the ratio of the walking speed to the walking frequency. Accordingly, for a given value for the wavelength, increasing of the span length will correspond to larger values of the response tending to those of a stationary system; this also depends on the structural damping [75–77].

The TFRF can be evaluated in both deterministic and probabilistic forms, and the two approaches are discussed in Sections 4.1 and 4.2, respectively. On the other hand, the deterministic and probabilistic check procedures will be presented in Section 5.

The sources of uncertainty and error were discussed in Sections 2.1 and 3. The interested reader is referred to [10] for a discussion on the sensitivity of footbridge vibrations to stochastic walking parameters.

4.1. Deterministic Approach. The modal response to a harmonic load crossing a beam at a constant speed can be obtained as the superposition of forced and of free-decay responses. Different authors derived the closed-form solution

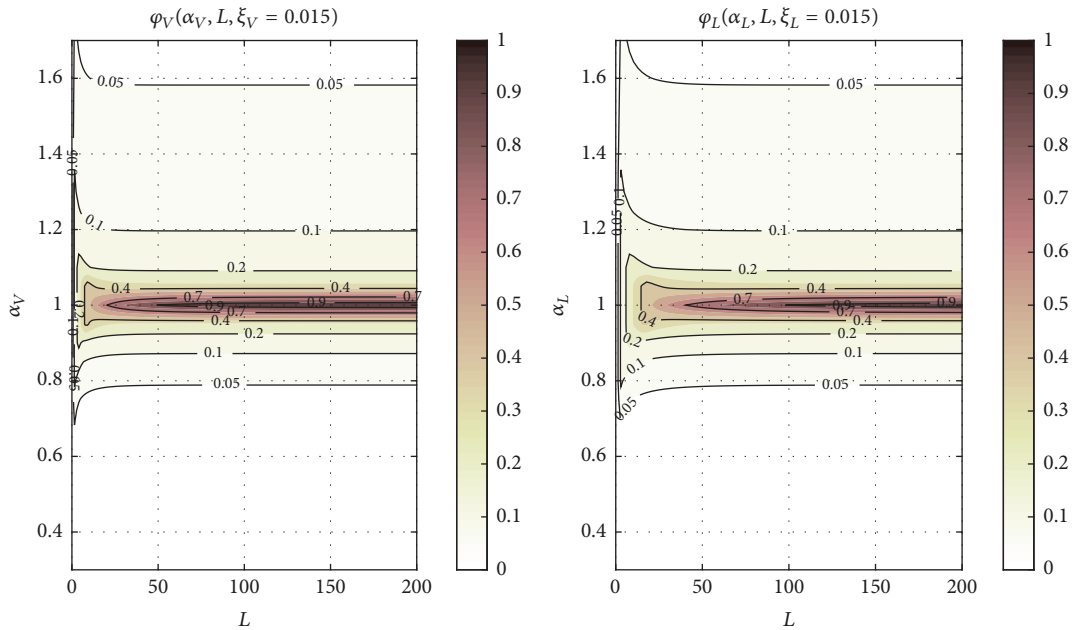

Figure 5: $\varphi_V(\alpha_V, L, \xi_V = 0.015)$ and $\varphi_L(\alpha_L, L, \xi_L = 0.015)$ for the simply supported beam evaluated using (19).

Table 2: Limits of validity and availability of closed-form peak modal response from different authors.

Reference	α	RL_i	Peak modal response
Abu-Hilal and Mohsen [74]	All	All	
Ricciardelli and Briatico [75]	All	0	√
Piccardo and Tubino [76]	1	All	√

to this problem. First, Abu-Hilal and Mohsen [74] derived a closed-form solution of the resonant and nonresonant response for any support condition. Subsequently, limited to the simply supported beam, Ricciardelli and Briatico [75] derived an approximated closed-form solution of the resonant and nonresonant response, together with a closed-form solution of the peak modal response. Then, Piccardo and Tubino [76] derived an approximated closed-form solution only of the resonant response, but for any support conditions, together with a closed-form solution of the peak modal response. A synthesis of the limits of validity and of the availability of closed-form peak modal response for different authors is reported in Table 2.

In the following, the case of a simply supported beam ($\mathrm{RL}_i = 0$) will be analyzed in Section 4.1.1, while the effects of the change of the support conditions will be described in Section 4.1.2.

4.1.1. Simply Supported Beam ($\mathrm{RL}_i = 0$). For the case of a simply supported beam, different closed-form solutions for the TFRF are available in the literature (see Table 2), and a comparison for the resonant case can be found in [5, 34]. The most accurate solution proves to be that of Ricciardelli and Briatico [75]:

$$\varphi_i\left(\mathrm{RL}_i = 0, \alpha_i, L, \xi_i\right) = \min \begin{cases} \xi_i \cdot \dfrac{2\alpha_i^2}{\left|1-\alpha_i^2\right|}\left[1 + \dfrac{1}{n_i}\dfrac{2}{\left|1-\alpha_i^2\right|} \cdot \exp\left[-\dfrac{\pi \cdot n_i(L) \cdot \xi_i}{2\alpha_i}\right]\right] \\ \dfrac{n_i(L) \cdot \xi_i}{1 + n_i^2(L) \cdot \xi_i^2}\left[\sqrt{1 + n_i^2(L) \cdot \xi_i^2} + \exp\left[-n_i(L) \cdot \xi_i\left(\dfrac{\pi}{2} + \arctan\dfrac{1}{n_i(L) \cdot \xi_i}\right)\right]\right], \end{cases} \tag{19}$$

where $n_i(L)$ is twice the number of load cycles imposed by the walker to the footbridge and is defined as

$$n_i(L) = \frac{2 \cdot \overline{f}_{w,i}}{\overline{v}} \cdot L = \begin{cases} 2.70\,\mathrm{m}^{-1} \cdot L & \text{for } i = V \\ 1.35\,\mathrm{m}^{-1} \cdot L & \text{for } i = L. \end{cases} \tag{20}$$

Equation (19) for the resonant case is quite consistent with that of Piccardo and Tubino [76].

An example of the vertical and lateral TFRF for $\xi_i = 0.015$ is shown in Figure 5, where it is visible that the maximum response is obtained for the resonant conditions. At resonance, the TFRF increases increasing the span length, due to the larger number of loading cycles. In particular, the TFRF increases with L only for relatively low values of L (around 20 m for $i = V$ and 40 m for $i = L$), while, for larger beam lengths, the TFRF remains constant. Out of resonance, the two figures are almost identical.

4.1.2. Effects of Different Support Conditions ($\mathrm{RL}_i > 0$). Change of support conditions influences mode shapes and thus acceleration response. In order to account for general support conditions, a boundary factor, BF_i, is defined as the ratio of the modal peak acceleration on beam with arbitrary RL_i to that of a simply supported beam (i.e., for $\mathrm{RL}_i = 0$):

$$\mathrm{BF}_i\left(\mathrm{RL}_i, \alpha_i, L, \xi_i\right) = \frac{\hat{\ddot{\eta}}_i\left(\mathrm{RL}_i, \alpha_i, L, \xi_i\right)}{\hat{\ddot{\eta}}_i\left(\mathrm{RL}_i = 0, \alpha_i, L, \xi_i\right)}. \tag{21}$$

Substituting (17) in (21), it can be observed that the boundary factor can be split into two parts:

$$\begin{aligned}\mathrm{BF}_i\left(\mathrm{RL}_i, \alpha_i, L, \xi_i\right) &= \mathrm{BF}_{m,i}\left(\mathrm{RL}_i\right) \cdot \mathrm{BF}_{\varphi,i}\left(\mathrm{RL}_i, \alpha_i, L, \xi_i\right) \\ &= \frac{m_i\left(\mathrm{RL}_i = 0\right)}{m_i\left(\mathrm{RL}_i\right)} \\ &\quad \cdot \frac{\varphi_i\left(\mathrm{RL}_i, \alpha_i, L, \xi_i\right)}{\varphi_i\left(\mathrm{RL}_i = 0, \alpha_i, L, \xi_i\right)},\end{aligned} \tag{22}$$

where $\varphi_i(\mathrm{RL}_i = 0, \alpha_i, L, \xi_i)$ and $m_i(\mathrm{RL}_i = 0)$ are the TFRF (see (19)) and the modal mass of a simply supported beam and $\varphi_i(\mathrm{RL}_i, \alpha_i, L, \xi_i)$ and $m_i(\mathrm{RL}_i)$ are those for a generic symmetric support conditions (i.e., arbitrary value of RL_i). The derivation of (22) is given in Appendix C.3. According to (22), $\mathrm{BF}_i(\mathrm{RL}_i, \alpha_i, L, \xi_i)$ accounts for the variation of modal mass through a mass boundary factor, $\mathrm{BF}_{m,i}(\mathrm{RL}_i)$, and of mode shape through a TFRF boundary factor, $\mathrm{BF}_{\varphi,i}(\mathrm{RL}_i, \alpha_i, L, \xi_i)$.

The variation of modal mass with RL_i, that is, $\mathrm{BF}_{m,i}(\mathrm{RL}_i)$, was shown in Figure 3 as $m_i(\mathrm{RL}_i)/m_i(\mathrm{RL}_i = 0)$, that is, the inverse of $\mathrm{BF}_{m,i}(\mathrm{RL}_i)$. This contribution only depends on the mode shape: with increasing RL_i, the modal mass reduces. The second term in (22), $\mathrm{BF}_{\varphi,i}(\mathrm{RL}_i, \alpha_i, L, \xi_i)$, depends on all the variables, as in (19).

Using the definition of $\mathrm{BF}_{\varphi,i}(\mathrm{RL}_i)$ given in (22), the TFRF for general support conditions can be expressed as

$$\begin{aligned}\varphi_i\left(\mathrm{RL}_i, \alpha_i, L, \xi_i\right) &= \mathrm{BF}_{\varphi,i}\left(\mathrm{RL}_i, \alpha_i, L, \xi_i\right) \\ &\quad \cdot \varphi_i\left(\mathrm{RL}_i = 0, \alpha_i, L, \xi_i\right).\end{aligned} \tag{23}$$

At resonance $\mathrm{BF}_i(\mathrm{RL}_i, \alpha_i = 1, L, \xi_i)$ can be evaluated using the solution of Piccardo and Tubino [76] while for nonresonant conditions the numerical solution of Abu-Hilal and Mohsen [74] must be used (see Table 2).

In the following, the trend of the boundary factor is only reported for the vertical direction for the sake of brevity, although similar conclusions apply to the case of lateral vibrations. The variation of $\mathrm{BF}_V(\mathrm{RL}_V, \alpha_V = 1, L, \xi_V = 0.015)$ (solid lines) and $\mathrm{BF}_{\varphi,V}(\mathrm{RL}_V, \alpha_V = 1, L, \xi_V = 0.015)$ (dashed lines) is shown in Figure 6 for RL_V equal to 0 (simply supported beam), 0.25, 0.5, 0.75, and 1 (clamped beam). The value of $\mathrm{BF}_{\varphi,V}$ increases with reducing rotational stiffness, $K_{r,V}$ (i.e., reducing RL_V). The increase of the modal peak acceleration with increasing RL_V (i.e., increasing $K_{r,V}$) is due to the choice of considering the mass per unit length, m, and the natural frequency, f_V, as input parameters. The latter result derives from having calculated the modal masses (i.e., $m_V(\mathrm{RL}_V)$ and $m_V(\mathrm{RL}_V = 0)$) starting from the same values of mass per unit length, m. Accordingly, for the same value of m, the increase of RL_V leads to a decrease of modal mass, m_V, as reported in Figure 3. The reduction of modal mass is followed by a reduction of stiffness of the beam, EI_V (see (8)), to keep f_V constant, being the frequency proportional to the ratio of the stiffness and modal mass. Accordingly, the reduction of stiffness brings an increase of the peak response, thus explaining the increase of $\mathrm{BF}_V(\mathrm{RL}_V, \alpha_V = 1, L, \xi_V)$ with increasing of RL_V.

On the other hand, if the modal mass, m_V (instead of the mass per unit length, m), and the natural frequency, f_V, are used as input parameters, the beam will be characterized by the same stiffness, EI_V, so as to have the same value of f_V. If the same modal mass is considered (i.e., $m_V(\mathrm{RL}_V)$ is the same for all RL_V), then $\mathrm{BF}_{m,V}(\mathrm{RL}_V) = 1$. Accordingly, the peak response is reduced with increasing RL_V, as intuitively it should behave. This can be observed looking only at the effect of RL_V on the TFRF, that is, $\mathrm{BF}_{\varphi,V}(\mathrm{RL}_V, \alpha_V = 1, L, \xi_V)$ (dashed line) in Figure 6, since $\mathrm{BF}_{m,V}(\mathrm{RL}_V) = 1$. In this case, the peak response reduction increases with increasing RL_V.

Away from resonance, the variation of $\mathrm{BF}_V(\mathrm{RL}_V = 1, \alpha_V, L, \xi_V = 0.015)$ is also shown in Figure 6. BF_V shows a marked dependence on L for $L \leq 50$ m, whereas it is almost constant for $L \geq 50$ m, especially away from resonance.

Finally, $\mathrm{BF}_i(\mathrm{RL}_i = 1, \alpha_i, L, \xi_i)$ for different values of ξ_i is reported in Appendix A for the vertical and lateral directions.

4.2. Probabilistic Approach. The PDF of the peak acceleration as a function of the footbridge characteristics (i.e., α_i, L, and ξ_i) is obtained through the convolution of the response for the vertical and lateral directions:

$$\begin{aligned}p_{\hat{\ddot{\eta}}_i}\left(\hat{\ddot{\eta}}_i\left(\alpha_i, L, \xi_i\right)\right) &= \int_0^\infty \int_0^\infty \int_0^\infty \int_0^\infty p_{\hat{\ddot{\eta}}_i, W, \mathrm{DLF}_i, \nu, f_{W,i}} \\ &\quad \cdot \mathrm{d}W \cdot d\mathrm{DLF}_i \cdot d\nu \cdot df_{w,i},\end{aligned} \tag{24}$$

where the PDF of the peak acceleration reported in the integral can be found applying the chain rule:

$$\begin{aligned}p_{\hat{\ddot{\eta}}_i, W, \mathrm{DLF}_i, \nu, f_{W,i}} &= p_{\hat{\ddot{\eta}}_i}\left(\hat{\ddot{\eta}}_i\left(\alpha_i, L, \xi_i\right) \mid W, \mathrm{DLF}_i, \nu, f_{w,i}\right) \\ &\quad \cdot p_W\left(W\right) \cdot p_{\mathrm{DLF}_i}\left(\mathrm{DLF}_i \mid f_{w,i}\right) \\ &\quad \cdot p_{f_{w,i}}\left(f_{w,i} \mid \nu\right) \cdot p_\nu\left(\nu\right),\end{aligned} \tag{25}$$

where $p_A(a \mid b)$ is the conditional probability of a given b. All the variables describing the SP (see Section 2.1) are statistically independent, except for ν and $f_{w,V}$. Accordingly, in the derivation of (25), only the conditional probability of $f_{w,i}$ given ν and DLF_V given $f_{w,V}$ was considered.

The multiple integral in (24) combined with (25) was solved through Monte Carlo simulations, using the following procedure in the vertical and lateral directions:

(1) Evaluation of the integral for $0.3 \leq \alpha_i \leq 1.7$ (step 0.1), $10\ \mathrm{m} \leq L \leq 200\ \mathrm{m}$ (step 10 m), and $0.001 \leq \xi_i \leq 0.015$ (step 0.001) and for $\mathrm{RL}_i = 0$ and 1

(2) Random generation of 10,000 walkers, whose characteristics (W, DLF_i, ν, and f_w) follow the PDFs of the SP of Section 2.1

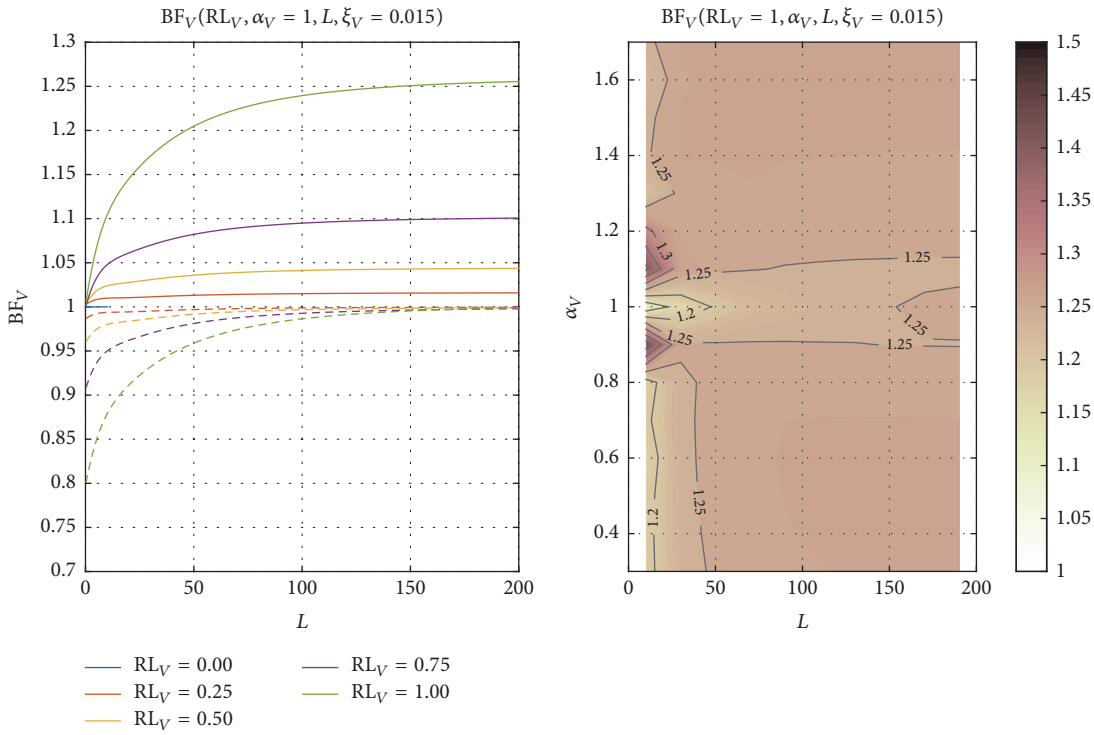

Figure 6: Boundary factor $\mathrm{BF}_V(\mathrm{RL}_V, \alpha_V = 1, L, \xi_V = 0.015)$ (solid lines) and TFRF boundary factor $\mathrm{BF}_{\varphi,V}(\mathrm{RL}_V, \alpha_V = 1, L, \xi_V = 0.015)$ (dashed lines) for different values of RL_V evaluated using the solution of Piccardo and Tubino [76]. $\mathrm{BF}_V(\mathrm{RL}_V = 1, \alpha_V, L, \xi_V = 0.015)$ evaluated numerically using the solution of Abu-Hilal and Mohsen [74].

(3) Evaluation of the modal vertical and lateral acceleration time histories, $\ddot{\eta}_i(t)$, for $\mathrm{RL}_i = 0$ and $\mathrm{RL}_i = 1$ using the model of Abu-Hilal and Mohsen [74] (see (12)) for the population of walkers generated in (2) (a time step of 0.01 s was used in the simulations)

(4) For each walker, evaluation of the lateral and vertical peak acceleration and evaluation of $\varphi_i(\mathrm{RL}_i, \alpha_i, L, \xi_i)$ (see (17))

(5) Evaluation of the empirical PDF of the TFRF, $p_{\varphi_i}(\varphi_i(\mathrm{RL}_i, \alpha_i, L, \xi_i))$

(6) Fit of the empirical PDF to a GEV distribution.

The distributions of the TFRF are fitted using the GEV distribution with the following CDF:

$$P_{\varphi_i}\left(\varphi_i\left(\mathrm{RL}_i, \alpha_i, L, \xi_i\right)\right) = \exp\left\{-\left[1 + k_i\left(\frac{\varphi_i - \mu_i}{\sigma_i}\right)\right]^{-1/k_i}\right\}, \quad (26)$$

where the location parameter, μ_i, the scale parameter, σ_i, and the shape parameter, k_i, are all dependent on RL_i, α_i, L, and ξ_i. A preliminary convergence study showed that the number of 10,000 simulations ensures a good accuracy and repeatability of the results.

The estimated GEV parameters for lateral and vertical vibrations for supported ($\mathrm{RL}_i = 0$) and clamped ($\mathrm{RL}_i = 1$) beams are shown in Appendix B. In all the cases investigated, the GEV parameters were found to depend on α_i and ξ_i, whereas a dependency on L was found only for $L \leq 20$ m for lateral vibrations and for $L \leq 40$ m for vertical vibrations. The explanation of this difference can be found observing the results of the deterministic approach reported in Section 4.1. Observing Figure 5, it can be seen that the variation of φ_i is noticeable up to 50 m while for larger values it is negligible. Accordingly, also the probabilistic model exhibits small variations of the GEV parameters for values of L associated with $L \leq 50$ m. In Appendix B, the GEV parameters are shown for $L = 10$ m, 20 m, 30 m, and 40 m and for L in excess of 50 m; the latter are the average value obtained varying L from 50 m to 200 m. In order to verify the accuracy of the mean GEV parameter representation, the STD of the GEV parameters in the range of L from 50 m to 200 m was calculated finding very low values of the standard deviation (compared with the values assumed by the variables reported in Appendix B): 1×10^{-2} for μ_i, 2×10^{-3} for σ_i, and 2×10^{-3} for k_i.

In all the cases investigated, k_i broadly ranges from −0.4 to 1.2 taking the largest values around resonance. Moreover, at resonance k_i slightly increases with decreasing structural damping, while it is approximately constant away from resonance. The maximum value of k_i is reached for $\alpha = 0.9$ for the lowest structural damping. k_i takes approximately the same values for RL = 0 and RL = 1. Globally, k_V takes larger values compared with k_L, with small exceptions. k_V is less dependent on damping than k_L. The variation of k_V and k_L with L is in agreement with the previous observations.

In all the cases investigated, σ_i and μ_i broadly range from 0 to 0.2 taking larger values at resonance and both increasing

Table 3: Probabilistic design values $\beta_D[P_D]$, after ISO 2394 [37].

Relative costs of safety measures	Consequences of failure			
	Small	Some	Moderate	Great
High	0 $[5 \cdot 10^{-1}]$	1.5 $[7 \cdot 10^{-2}]$	2.3 $[1 \cdot 10^{-2}]$	3.1 $[1 \cdot 10^{-3}]$
Moderate	1.3 $[1 \cdot 10^{-1}]$	2.3 $[1 \cdot 10^{-2}]$	3.1 $[1 \cdot 10^{-3}]$	3.8 $[7 \cdot 10^{-5}]$
Low	2.3 $[1 \cdot 10^{-2}]$	3.1 $[1 \cdot 10^{-3}]$	3.8 $[7 \cdot 10^{-5}]$	4.3 $[8 \cdot 10^{-6}]$

with damping. Globally, σ_L is larger than σ_V for $\alpha_i > 1$ especially for low damping, and the two quantities are quite similar for $\alpha_i < 1$. For both vertical and lateral directions, both σ_i and μ_i are larger for the clamped case than for the supported case; this is in agreement with the variation of BF_i (Figures 7 and 8). The same observations can be made regarding the dependence on L of σ_i and μ_i, as those made for k_i.

5. Reliability Analysis: Deterministic and Probabilistic Approaches

In this section, first (deterministic) and third (probabilistic) level safety assessments methods will be applied. In particular, it is assessed that the acceleration induced by the crossing of a walker is not causing loss of comfort for a receiver.

In the application of the first level safety assessment method, it is assumed that the basic variables are summarized into a deterministic value of capacity (the maximum tolerable acceleration), C_i, and a deterministic value of demand (the peak acceleration induced by a single walker), D_i. Capacity and demand are expressed in terms of TFRFs:

$$D_i = \varphi_i\left(\mathrm{RL}_i, \alpha_i, L, \xi_i\right) \le \varphi_{i,\max} = C_i \quad \forall i, \tag{27}$$

where D_i is expressed as in (23) and the limit acceleration is expressed in terms of equivalent TFRF:

$$\begin{aligned} C_i &= \varphi_{i,\max} \\ &= \left(\mathrm{BF}_{m,i}\left(\mathrm{RL}_i\right) \cdot \frac{\overline{\mathrm{DLF}_i} \cdot \overline{W}}{2\xi_i} \cdot \frac{1}{m_i}\right)^{-1} \hat{\ddot{\eta}}_{i,\max}, \end{aligned} \tag{28}$$

where m_i is the modal masses evaluated considering $\mathrm{RL}_i = 0$ (simply supported beam), $\mathrm{BF}_{m,i}(\mathrm{RL}_i)$ is the mass boundary factor correcting the modal masses for support condition, and $\hat{\ddot{\eta}}_{i,\max}$ is the maximum tolerable acceleration.

Application of the third level method requires either numerical integration or approximate analytical methods (such as first- and second-order reliability methods) or simulation methods [78]; the latter was used in this study (Section 4.2). Given the Joint Probability Density Function (JPDF), $p_{C,D}(c, d)$, of capacity and demand, then the probability of failure $P_{\mathrm{fail},i}$ is given as

$$P_{\mathrm{fail},i} = \int_{C-D\le 0} p_{C_i,D_i}\left(c_i, d_i\right) \cdot \mathrm{d}c_i \cdot \mathrm{d}d_i. \tag{29}$$

C_i has a negligible variability compared to D_i; then it is reasonable to consider it as deterministic. Under this assumption, $P_{\mathrm{fail},i}$ can be evaluated as the Complementary Cumulative Distribution Function (CCDF):

$$P_{\mathrm{fail},i} = 1 - \int_0^{\varphi_{i,\max}} p_{\varphi_i}\left(\varphi_i\left(\mathrm{RL}_i, \alpha_i, L, \xi_i\right)\right) \cdot \mathrm{d}\varphi_i, \tag{30}$$

where the integration limit is equal to the maximum tolerable acceleration reported in the capacity value (see (28)).

Equivalently, the reliability index can be considered:

$$\beta_i = -\Phi_U^{-1}\left(P_{\mathrm{fail},i}\right), \tag{31}$$

where Φ_U^{-1} denotes the inverse standardized normal distribution function.

The acceptance condition is based on the requirement that the probability of failure does not exceed the design value $P_{D,i}$, or that the reliability index is greater than its corresponding design value $\beta_{D,i} = -\Phi_U^{-1}(P_{D,i})$ [37]:

$$\begin{aligned} P_{\mathrm{fail},i} \le P_{D,i} &\Longleftrightarrow \\ \beta_i \ge \beta_{D,i}&. \end{aligned} \tag{32}$$

In Eurocode 0 [36] and ISO 2394 [37], reliability requirements are expressed in terms of the reliability index β_D; these are related to the expected social and economic consequences. In particular, ISO 2394 [37] gives the probabilistic design values as a function of the relative costs of safety measures and of the consequence of failure (Table 3).

The consequence classes in Table 3 are quantified through the ratio between the failure costs and the costs of construction. In the case of footbridge vibrations, the consequence of vibrations is small, as no damage to things or people occurs. ISO 2394 [37] suggests $\beta_D = 0$ $[P_D = 5 \cdot 10^{-1}]$ for reversible limit states (Table 3). However, based on performance demand and on the outcome of cost-benefit analyses, the designer may find it appropriate to increase or reduce the probabilistic design values, that is, to increase or reduce reliability. As reported by ISO 2394 [37], the probabilistic design values are *"formal or notional numbers, intended primarily as a tool for developing consistent design rules, rather than giving a description of the structural failure frequency."* In the same manner, Eurocode 0 [36] gives a target reliability index β_D of 1.5 for serviceability irreversible limit state not providing any indication for the serviceability reversible one.

For both levels of assessment (deterministic and probabilistic), it is necessary to quantify capacity, that is, to set the maximum tolerable acceleration; reference values can be found in the literature [8]. The interested reader is also referred to [79, 80] for further information. ISO 10137 [27] states that *"the designer shall decide on the serviceability*

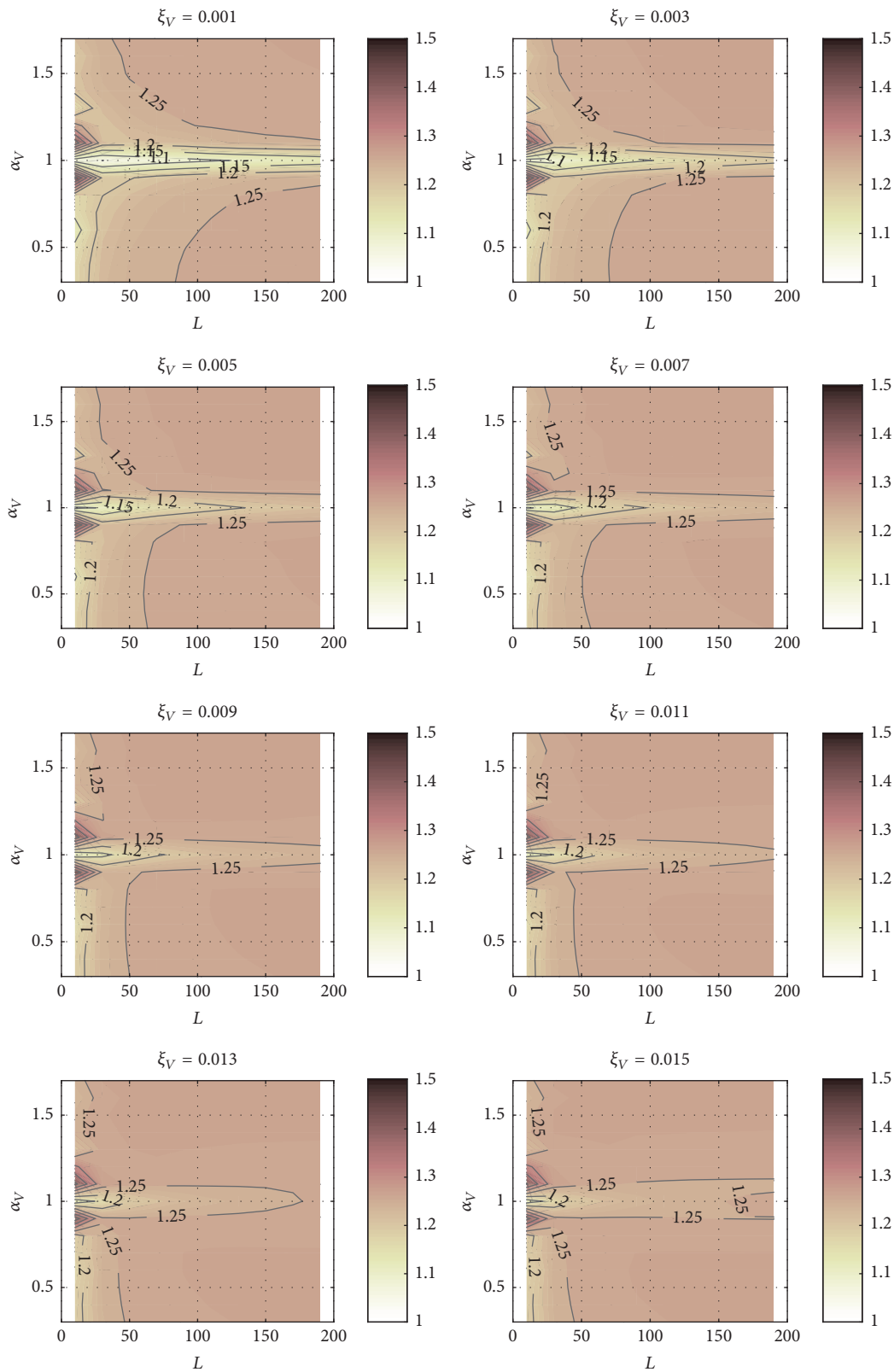

FIGURE 7: $\mathrm{BF}_V(\mathrm{RL}_V = 1, \alpha_V, L, \xi_V)$ for different values of ξ_V numerically evaluated using the solution of Abu-Hilal and Mohsen [74].

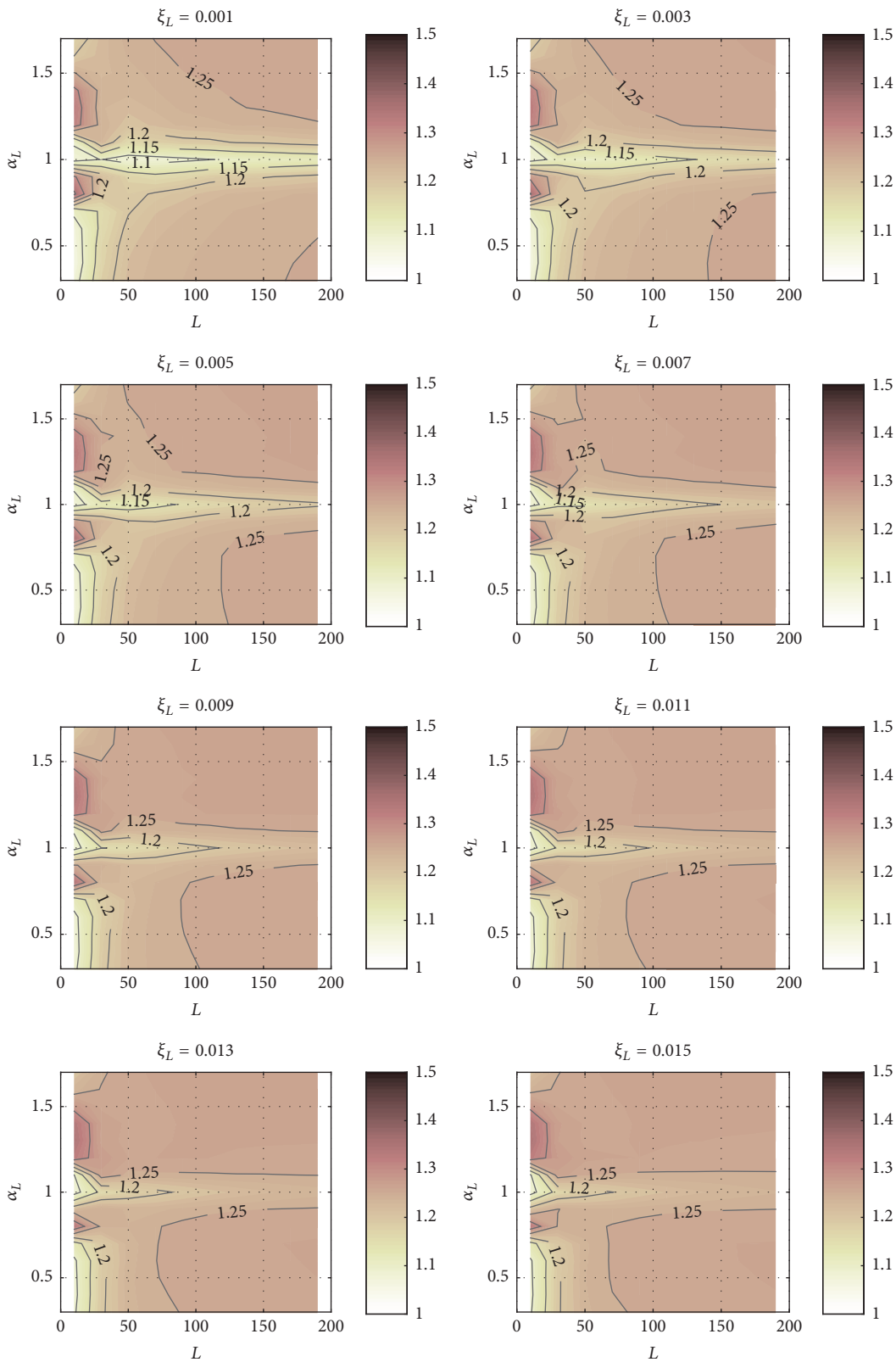

FIGURE 8: $BF_L(RL_L = 1, \alpha_L, L, \xi_L)$ for different values of ξ_L numerically evaluated using the solution of Abu-Hilal and Mohsen [74].

criterion and its variability." Further, ISO 10137 [27] states that footbridges "*shall be designed, so that vibration amplitudes from applicable vibration sources do not alarm potential users.*" In particular, Annex C to ISO 10137 [27] provides limiting criteria for human comfort on footbridges in the range of frequency of 1 to 80 Hz. The capacity is expressed in terms of RMS acceleration evaluated on a 1 s window (running RMS method, ISO 2631 [81]); the limit values are given as a function of the vibration frequency (base curves), for the lateral (side to side and back to chest) and vertical directions. For footbridges, the base curves must be multiplied by a factor of 30 in the vertical directions and by a factor of 60 in the lateral direction. The factor of 30 applies only to pedestrians standing still on the bridge, because sensitivity to vibration decreases when walking. Finally, the results of the numerical simulations show that, for the range of the input parameters considered, the ratio between the peak values and the 1 s RMS peak values of the acceleration (Maximum Transient Vibration Value, ISO 2631 [81]) is around $\sqrt{2}$ (1.13 to 1.57 in the lateral direction and 1.30 to 1.51 in the vertical direction), similar to the peak factor of a stationary sinusoidal process.

The maximum tolerable acceleration is therefore evaluated from the ISO 10137 base curves:

$$\begin{aligned}\hat{\ddot{\eta}}_{V,\max}(\alpha_V) &= \sqrt{2}\cdot 30\cdot \hat{\ddot{\eta}}_{V,\mathrm{rms}}(\alpha_V)\\ &= \begin{cases} 0.21 & \text{if } \alpha_V \le 0.47\\ 0.140 + 0.150\cdot\alpha_V & \text{if } \alpha_V > 0.47,\end{cases}\\ \hat{\ddot{\eta}}_{L,\max}(\alpha_L) &= \sqrt{2}\cdot 60\cdot \hat{\ddot{\eta}}_{L,\mathrm{rms}}(\alpha_L)\\ &= \begin{cases} 12.52 - 25.75\cdot\alpha_L & \text{if } \alpha_L \le 0.47\\ 0.30 & \text{if } \alpha_L > 0.47,\end{cases}\end{aligned} \tag{33}$$

where $\hat{\ddot{\eta}}_{V,\max}(\alpha_V)$ and $\hat{\ddot{\eta}}_{L,\max}(\alpha_L)$ are the peak acceleration thresholds and $\hat{\ddot{\eta}}_{V,\mathrm{rms}}(\alpha_V)$ and $\hat{\ddot{\eta}}_{L,\mathrm{rms}}(\alpha_L)$ are the corresponding 1 s RMS peak acceleration thresholds (base curves) in m/s^2. The acceleration thresholds are given in terms of generalized coordinates (i.e., $\hat{\ddot{\eta}}_{V,\max}(\alpha_V)$ and $\hat{\ddot{\eta}}_{L,\max}(\alpha_L)$), which applies to the case where mode shapes are normalized to one (Section 3).

Equations (33) are shown in Figure 9, limited to the frequency range of interest for footbridges. For $\alpha_L \ge f_{w,L}$ (i.e., $f_L \le 1$ Hz), the acceleration threshold has been extrapolated to a constant value. For the resonant case, where the acceleration is larger, the vertical and lateral acceleration thresholds are similar and equal to $\hat{\ddot{\eta}}_{V,\mathrm{rms}}(\alpha_V = 1) = 0.29\,\mathrm{m/s^2}$ and $\hat{\ddot{\eta}}_{L,\mathrm{rms}}(\alpha_L = 1) = 0.30\,\mathrm{m/s^2}$, respectively. In the vertical direction, $\hat{\ddot{\eta}}_{V,\mathrm{rms}}(\alpha_V)$ increases in almost the entire range of α_V. In the lateral direction, $\hat{\ddot{\eta}}_{L,\mathrm{rms}}(\alpha_L)$ is taken as constant for $\alpha_L \ge 0.47$ and strongly increases for $\alpha_L < 0.47$ reducing the risk of loss of comfort.

6. Application to a Steel Truss Footbridge

As an example, the proposed procedure is applied to a prototype steel truss footbridge with an overall length of 101.90 m (central span of 90.00 m with two lateral cantilevers of 6.20 m and 5.70 m, resp.), a width of 3.50 m, and a height of truss of 4.45 m. The structural members, designed according to the Italian Code provisions [82], are made of grade S355 steel.

Table 4: Dynamic characteristics of the truss footbridge. m_V and m_L are evaluated considering a simply supported beam; that is, $\mathrm{RL}_i = 0$.

Variable	Dimension	$i = V$	$i = L$
L	[m]	90	
m	[kg/m]	1,495	
m_i	[kg]	67,275	67,275
ξ_i	[%]	0.5	0.5
α_i	[–]	1.061	0.507
RD_i	[–]	2.694	0.357
RL_i	[–]	0.48	0.975
BF_i	[–]	1	1.21
$\mathrm{BF}_{m,i}$	[–]	1	1.25
$\mathrm{BF}_{\varphi,i} = (\mathrm{BF}_i/\mathrm{BF}_{m,i})$	[–]	1	0.97

The footbridge was modeled using the FE software package SAP2000 [83] as a 3D truss beam simply supported at four nodes. In particular, fixed bearings were placed on one side of the beam and longitudinally sliding bearings on the other side. The mean mass per unit of length of the footbridge is 1,495 kg/m corresponding to a modal mass of 67,275 kg in both directions, considering simply support ($\mathrm{RL}_i = 0$) conditions. Damping ratio was set to 0.5% in both directions. Modal analysis was performed, and the first two modes of vibration were found to be the first vertical bending mode ($f_V = 1.789$ Hz) and the first lateral bending mode ($f_L = 1.873$ Hz), respectively (Figure 10). The natural frequencies correspond to $\alpha_V = 1.06$ and $\alpha_L = 0.51$, both indicating possible walking-induced vibrations.

To evaluate the actual support condition in terms of RL_i using (16), evaluation of RD_i defined through (15) is required; this was done by applying a uniform load in lateral and vertical directions to the FE model and evaluating the corresponding end rotation θ_i and midspan deflection δ_i. It should be pointed out that the uniform load coming from the deck is allocated to the nodes of the FE model using a tributary area load criterion. Finally, RD_i was converted into an equivalent RL_i using (16). A synthesis of the footbridge dynamic characteristic is given in Table 4. The RL (Table 4) correspond to a clamped beam in the lateral direction and to an intermediate condition between the simply supported and clamped beam for the vertical direction. In this application, considering that the boundary factor corresponding to $\mathrm{RL}_i = 0.5$ is quite similar to that corresponding to $\mathrm{RL}_i = 0$ (Figure 6), the condition $\mathrm{RL}_L = 1$ is used for the lateral direction and $\mathrm{RL}_V = 0$ for the vertical direction. The last assumption is also made because the procedure proposed in this study is only given for $\mathrm{RL}_i = 0$ and $\mathrm{RL}_i = 1$. The variation of the support conditions with respect to the simply supported case in the lateral direction makes it necessary to evaluate BF_L, $\mathrm{BF}_{m,L}$, and $\mathrm{BF}_{\varphi,L}$. In particular, from Figure 8 one can find $\mathrm{BF}_L = 1.21$, while $\mathrm{BF}_{m,L} = 1.25$ was found from Figure 3. Moreover, $\mathrm{BF}_{\varphi,L} = 0.968$ was estimated dividing BF_L by $\mathrm{BF}_{m,L}$ using the definition of (22).

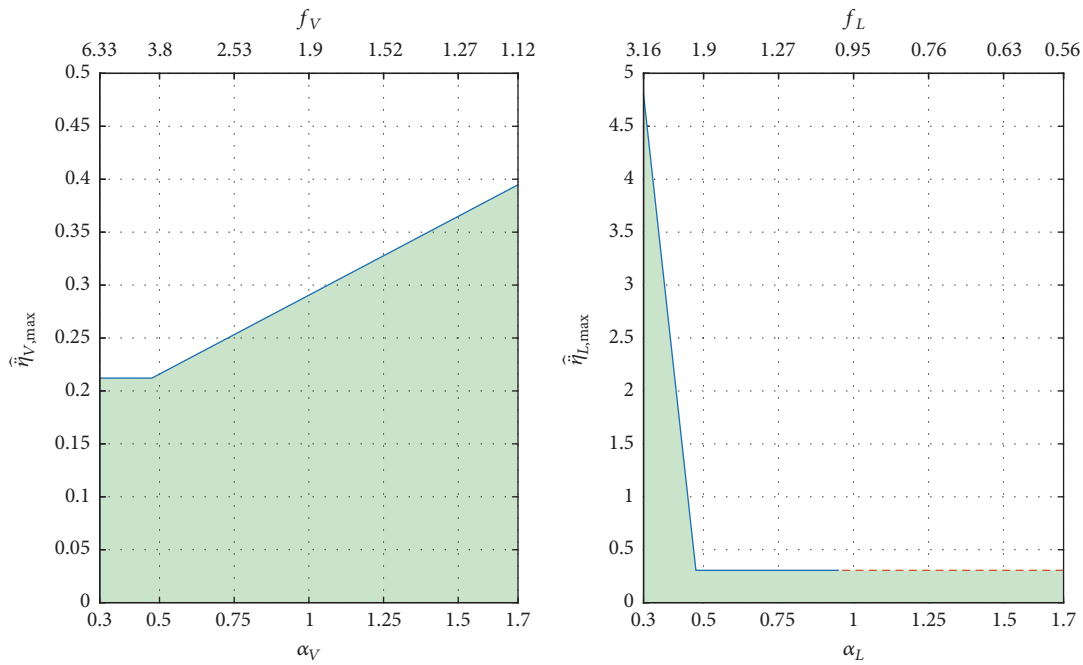

Figure 9: Threshold vertical and lateral peak acceleration using (33). The red dashed line indicates extrapolated values for $f_L \leq 1$ Hz. Green areas indicate the region of acceptable comfort.

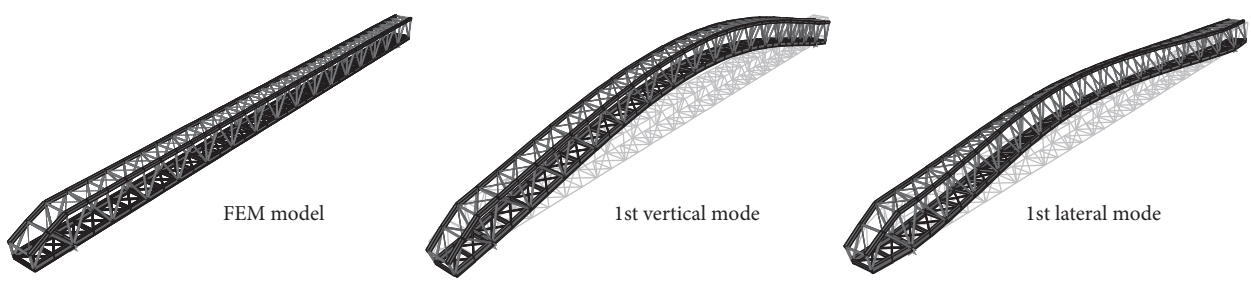

Figure 10: 3D SAP2000 Finite Element model of the truss footbridge, and first lateral and vertical mode shapes.

The limit acceleration was calculated according to ISO 10137 [27] using (33) (see Figure 9) and the design value of P_D and β considering small consequences of failure and moderate relative costs of safety measures according to ISO 2394 [37] (see Table 3). For both, vertical and lateral directions,

$$\begin{aligned} \hat{\hat{\eta}}_{\max} &= 0.3\,\mathrm{m/s^2}, \\ P_D &= 0.1, \\ \beta_D &= -\Phi_U^{-1}\left(P_D\right) = 1.3. \end{aligned} \tag{34}$$

The acceleration capacity is expressed in terms of equivalent TFRFs using (28):

$$\begin{aligned} C_V &= \left(\mathrm{BF}_{m,V} \cdot \frac{\overline{\mathrm{DLF}}_V \cdot \overline{W}}{2\xi_V} \frac{1}{m_V}\right)^{-1} \cdot \hat{\hat{\eta}}_{V,\max} = 0.775, \\ C_L &= \left(\mathrm{BF}_{m,L} \cdot \frac{\overline{\mathrm{DLF}}_L \cdot \overline{W}}{2\xi_L} \frac{1}{m_L}\right)^{-1} \cdot \hat{\hat{\eta}}_{L,\max} = 5.723. \end{aligned} \tag{35}$$

The acceleration demand TFRFs are evaluated for the simply supported beam using (19), and these values are corrected to account for the mode shape using BF as reported in (23):

$$\begin{aligned} D_V &= \varphi_V\left(\mathrm{RL}_V, \alpha_V, L, \xi_V\right) = 1 \cdot 0.0904 = 0.0904, \\ D_L &= \varphi_L\left(\mathrm{RL}_L, \alpha_L, L, \xi_L\right) = 0.97 \cdot 0.0035 = 0.0034. \end{aligned} \tag{36}$$

The deterministic check is performed using the inequality condition expressed in (27):

$$\begin{aligned} D_V &= 0.0904 < 0.775 = C_V, \\ D_L &= 0.0034 < 5.723 = C_L. \end{aligned} \tag{37}$$

Using the deterministic approach, it is found that maximum acceleration induced by the SW is lower than the acceptable threshold. In the lateral direction, the demand is much smaller than the capacity indicating large reliability. Conversely, in the vertical direction, the demand and the capacity are closer showing lower safety.

The probabilistic reliability analysis is based on the definition of the GEV parameters (see (26)); these are given in Appendix B. The lateral GEV parameters are evaluated considering $\mathrm{RL}_L = 1$ and using Figure 11, whereas the vertical GEV parameters are evaluated considering $\mathrm{RL}_V = 0$ and using Figure 12:

$$\begin{aligned} k_V\left(\mathrm{RL}_V = 0, \alpha_V, L, \xi_V\right) &= 0.6718, \\ \mu_V\left(\mathrm{RL}_V = 0, \alpha_V, L, \xi_V\right) &= 0.05067, \\ \sigma_V\left(\mathrm{RL}_V = 0, \alpha_V, L, \xi_V\right) &= 0.05588, \\ k_L\left(\mathrm{RL}_L = 1, \alpha_L, L, \xi_L\right) &= -0.0129, \\ \mu_L\left(\mathrm{RL}_L = 1, \alpha_L, L, \xi_L\right) &= 0.001828, \\ \sigma_L\left(\mathrm{RL}_L = 1, \alpha_L, L, \xi_L\right) &= 0.003309. \end{aligned} \tag{38}$$

The value of the CDF corresponding to TFRF predicted using the deterministic procedure (i.e., (36)) is equal to

$$\begin{aligned} P_{\varphi_V}\left(D_V\right) &= 0.565, \\ P_{\varphi_L}\left(D_L\right) &= 0.379. \end{aligned} \tag{39}$$

The PDF and CDF of φ_i for the vertical and lateral direction evaluated using the GEV parameters reported in (38) are shown in Figure 13, together with the deterministic acceleration demand TFRFs (see (36)). This result shows that, using the SW (i.e., walker having the mean characteristics of the SP), the cumulative probability is either higher or lower than the median of the probability distribution. In other words, this means that using mean characteristics of the SP characteristics can lead to unconservative evaluations as the obtained probability of exceeding can be different from the median, that is, 0.5.

$P_{\mathrm{fail},i}$ can be evaluated as the Complementary Cumulative Distribution Function (CCDF) associated with a TFRF equal to either C_V or C_L:

$$\begin{aligned} P_{\mathrm{fail},V} &= 0.0296 \Longleftrightarrow \\ \beta_V &= 1.887, \\ P_{\mathrm{fail},L} &\longrightarrow 0.0 \Longleftrightarrow \\ \beta_L &\longrightarrow \infty. \end{aligned} \tag{40}$$

The 0 probability of failure in the lateral direction of (40) is due to the negative values of k_L (see (38)) leading to a reversed Weibull distribution that is characterized by an upper limit. Accordingly, also the reliability index assumes infinitive value.

The acceptance condition is based on a requirement that the probability of failure $P_{\mathrm{fail},i}$ does not exceed the design value $P_{D,i}$ or the reliability index β_i is greater than its design value $\beta_{D,i}$ [37]:

$$\begin{aligned} P_{\mathrm{fail},V} &= 0.0296 < 0.1 = P_{D,V} \Longleftrightarrow \\ \beta_V &= 1.887 > 1.3 = \beta_D, \\ P_{\mathrm{fail},L} &= 0.0 < 0.1 = P_{D,L} \Longleftrightarrow \\ \beta_L &= \infty > 1.3 = \beta_D. \end{aligned} \tag{41}$$

Application of the probabilistic approach shows that the probability of failure is lower than the design probability. In particular, in the lateral direction, the check is satisfied in all cases (it can be considered a deterministic safety condition), while in the vertical direction the ratio between the capacity and the demand is lower. Approximately in 2.96% (see (40)) of the cases, the vertical acceleration induced by a single walker crossing the footbridge is larger than the threshold value.

7. Conclusions

Prior work has evaluated the dynamic effects induced by a single walker crossing a footbridge. The research available focuses on the definition of force characteristics and on the related dynamic response. No complete procedure is available for the probabilistic assessment of footbridges against the crossing of single walkers.

In this paper, a procedure for the deterministic and probabilistic assessment of footbridges against the crossing of single walkers was presented. This scenario is considered by different standards and design guidelines, such as ISO 10137. The procedure presented complies with Eurocode 0 [36] and ISO 2394 [37] and allows controlling the reliability level. The flow diagram of the procedure is given in Figure 4. First, the definition of the walker and footbridge dynamic characteristics is needed: a study of the data available in the literature allowed the definition of a Standard Population of walkers. Only walking conditions were considered. The common beam-type footbridge characteristics were evaluated and a dynamic modal model according to Abu-Hilal and Mohsen [74] was presented. All the variables defining the footbridge characteristics were chosen as such to obtain a simple procedure suitable for design implementation. The peak acceleration was chosen as the engineering demand parameter and it was derived with both a deterministic and a probabilistic approach. Using the deterministic approach, the serviceability check is carried out comparing the peak acceleration induced by a walker having the mean characteristics of the Standard Population, with the acceleration thresholds of ISO 10137 [27]. With the probabilistic approach, the exceedance probability of the threshold acceleration must be lower than the reliability levels defined in ISO 2394 [37]. This study, therefore, indicates that the use of the deterministic approach without the knowledge of the real reliability levels can lead to unconservative evaluations. Finally, application of deterministic and probabilistic approaches to a prototype steel footbridge showed how it can be easily used in the engineering practice.

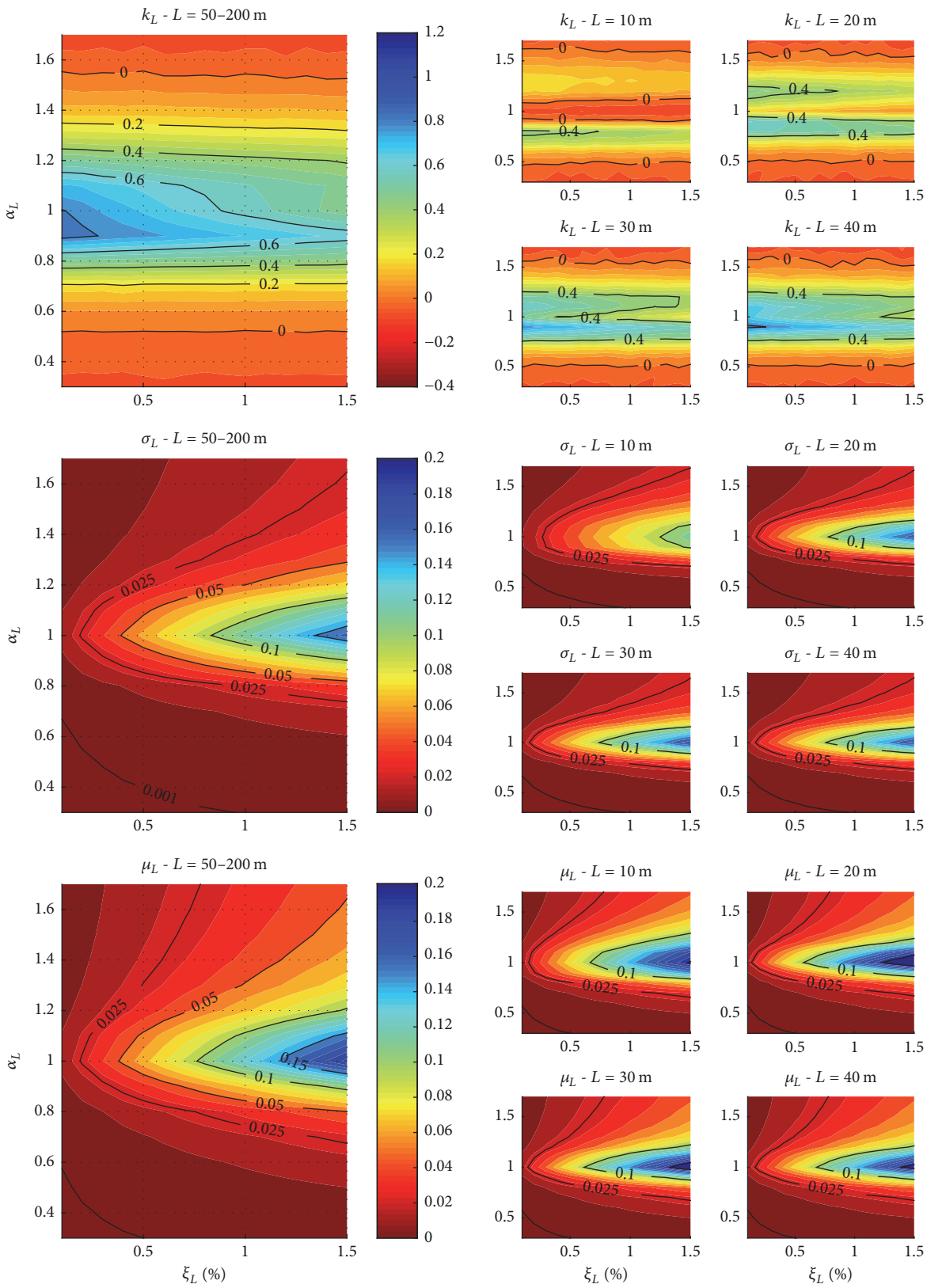

FIGURE 11: GEV parameters of $P_{\varphi_L}(\varphi_L(\mathrm{RL}_L = 1, \alpha_L, L, \xi_L))$: double clamped case in lateral direction.

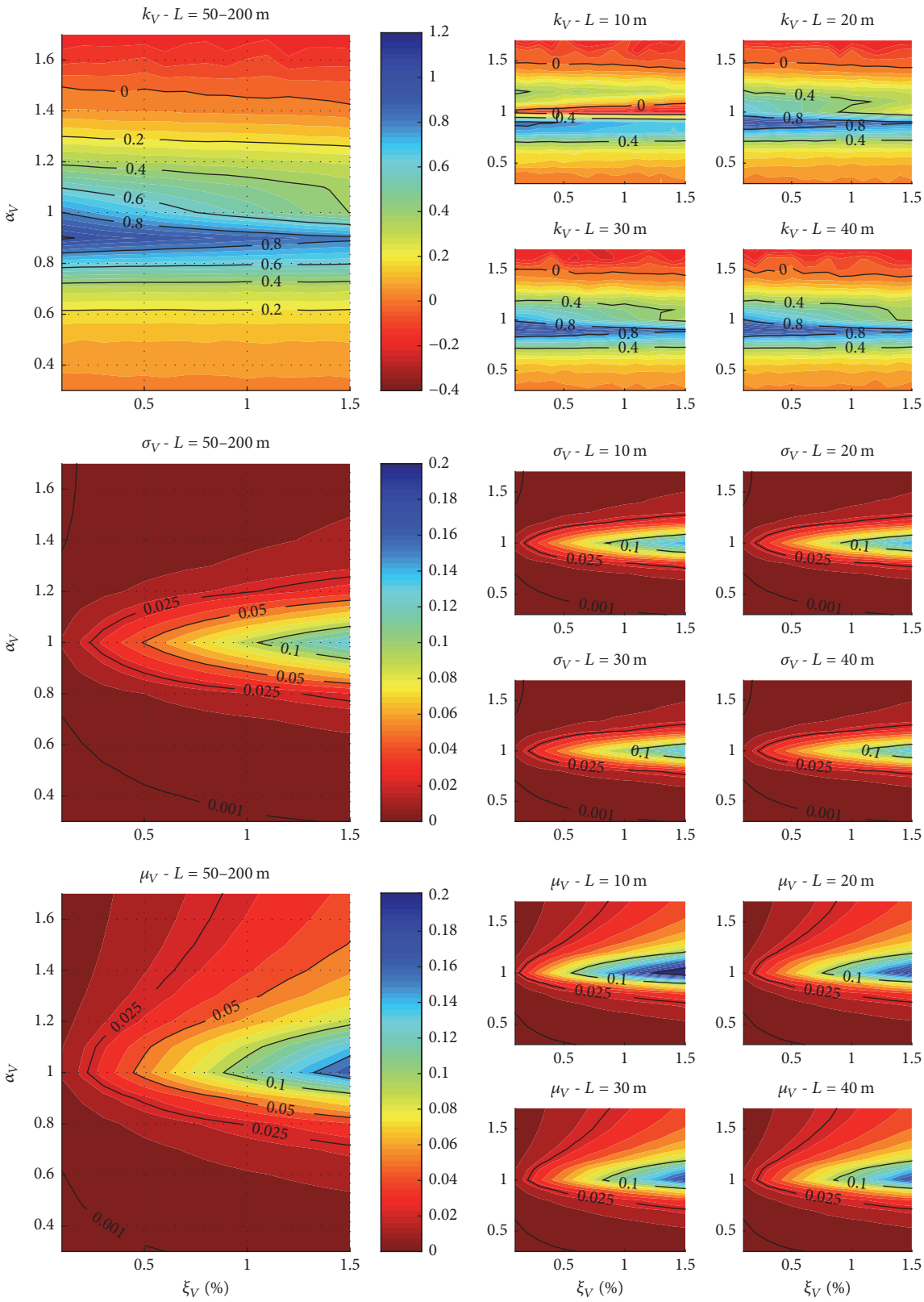

FIGURE 12: GEV parameters of $P_{\varphi_V}(\varphi_V(\mathrm{RL}_V = 0, \alpha_V, L, \xi_V))$: simply supported case in vertical direction.

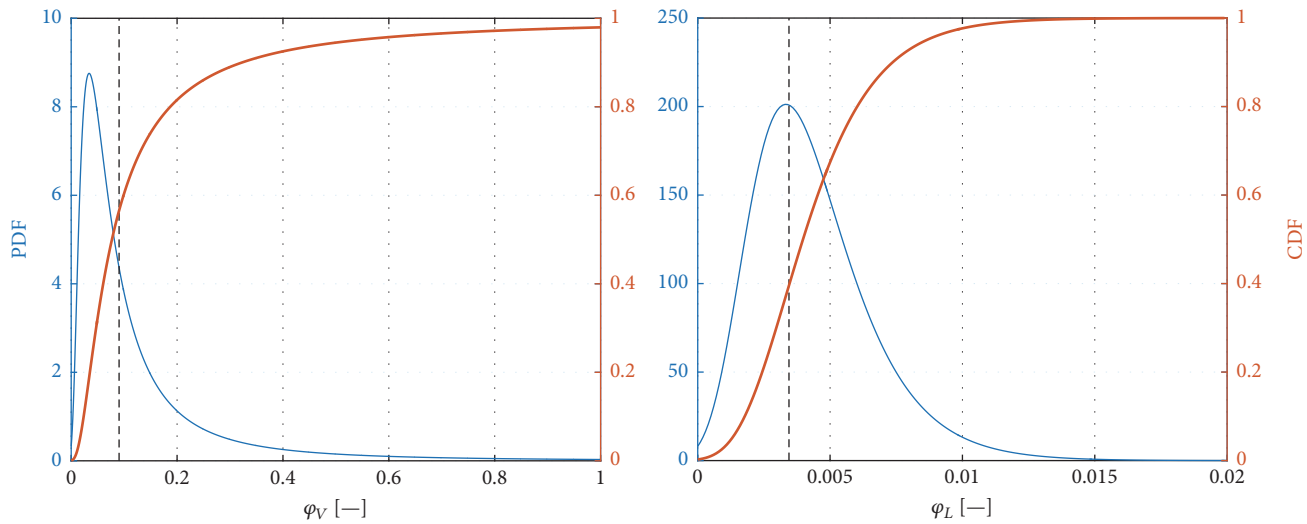

Figure 13: Probability Density Function (PDF, thin line) and Cumulated Distribution Function (CDF, thick line) of φ_i for the vertical and lateral direction (GEV parameters are reported in (38)). The vertical dashed line indicates the deterministic acceleration demand TFRFs, D_V and D_L (see (36)).

Appendix

A. Boundary Factor for the Clamped Case RL = 1

See Figures 7 and 8.

B. GEV Parameters for RL = 1 and RL = 0

See Figures 15 and 11 for RL = 1. See Figures 12 and 14 for RL = 0.

C. Derivation of (14), (16), and (22)

C.1. Derivation of (14). Let us consider a beam supported at both ends by fixed vertical constraints and with variable rotational stiffness (Figure 2). In this study, only symmetric support conditions will be considered:

$$K_{r,1,i} = K_{r,2,i} = K_{r,i}, \tag{C.1}$$

where the subscript $i = V, L$ indicates the vertical and lateral direction, respectively. The following derivation will be done for a generic direction i.

If we consider the beam loaded by an arbitrary symmetric load, the rotation at the two ends will be the same:

$$\Theta_{1,i} = \Theta_{2,i} = \Theta_i. \tag{C.2}$$

Let us define a nondimensional restrained level (RL_i), defined as the ratio of the end moment for the particular support condition (i.e., value of $K_{r,i}$) due to an arbitrary symmetric load, $M_i(K_{r,i})$, to that of the clamped beam subjected to the same load, $M_i(K_{r,i} \to \infty)$:

$$\mathrm{RL}_i \equiv \frac{M_i(K_{r,i})}{M_i(K_{r,i} \to \infty)} = \frac{M_i(\mathrm{RL}_i)}{M_i(\mathrm{RL}_i \to 1)}. \tag{C.3}$$

Therefore, RL_i is in the range of 0 (supported case, $K_{r,i} = 0$) to 1 (clamped case, $K_{r,i} \to \infty$). The bending moment at the two ends can be expressed according to

$$\begin{aligned} M_i(\mathrm{RL}_i) &= K_{r,i}(\mathrm{RL}_i) \cdot \Theta_i(\mathrm{RL}_i) \\ &= \mathrm{RL}_i \cdot M_i(\mathrm{RL}_i \longrightarrow 1). \end{aligned} \tag{C.4}$$

Using the assumptions of symmetric load and boundary conditions, the rotation at the end for a generic value of RL_i, $\Theta_i(\mathrm{RL}_i)$, can be written as

$$\begin{aligned} \Theta_i(\mathrm{RL}_i) &= \Theta_i(\mathrm{RL}_i = 0) - \frac{M_i(\mathrm{RL}_i) L}{3EI_i} - \frac{M_i(\mathrm{RL}_i) L}{6EI_i} \\ &= \Theta_i(\mathrm{RL}_i = 0) - \frac{M_i(\mathrm{RL}_i) L}{2EI_i}, \end{aligned} \tag{C.5}$$

where $\Theta_i(\mathrm{RL}_i = 0)$ is the rotation at one end of a simply supported beam and $M_i(\mathrm{RL}_i)$ is the bending moment at one end (the two bending moments at the two ends are the same due to the symmetry in the load and constraints).

Substituting (C.4) in (C.5), the following can be obtained:

$$\begin{aligned} \Theta_i(\mathrm{RL}_i) &= \Theta_i(\mathrm{RL}_i = 0) - \frac{M_i(\mathrm{RL}_i) L}{2EI_i} \\ &= \Theta_i(\mathrm{RL}_i = 0) - \frac{K_{r,i} \cdot \Theta_i(\mathrm{RL}_i) \cdot L}{2EI_i}. \end{aligned} \tag{C.6}$$

Then, solving by $\Theta_i(\mathrm{RL}_i)$, the following relation as a function of $K_{r,i}$ can be found:

$$\Theta_i(\mathrm{RL}_i) = \Theta_i(\mathrm{RL}_i = 0) \cdot \left(1 + \frac{2EI_i}{K_{r,i} \cdot L}\right). \tag{C.7}$$

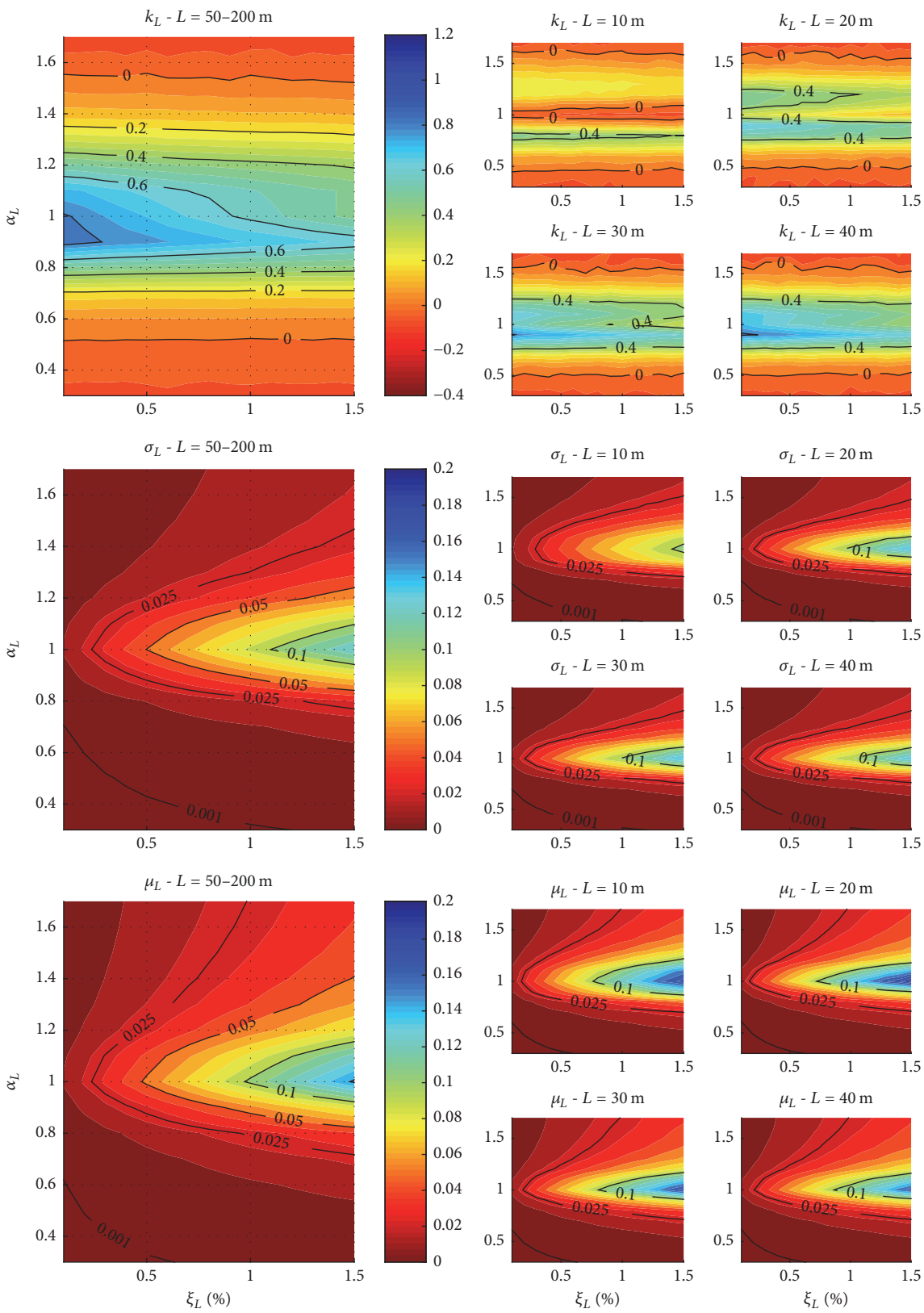

Figure 14: GEV parameters of $P_{\varphi_L}(\varphi_L(\mathrm{RL}_L = 0, \alpha_L, L, \xi_L))$: simply supported case in lateral direction.

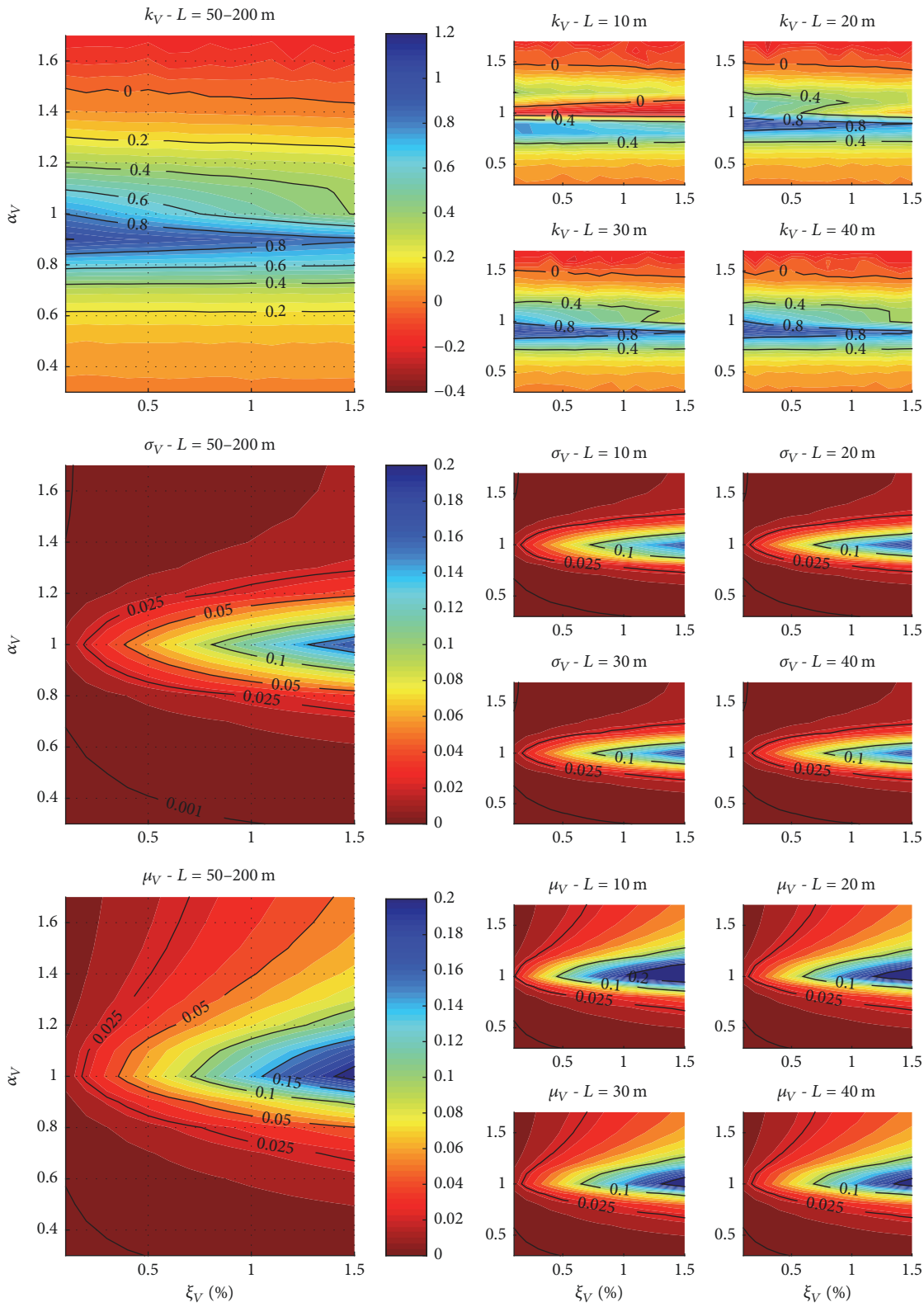

FIGURE 15: GEV parameters of $P_{\varphi_V}(\varphi_V(\mathrm{RL}_V = 1, \alpha_V, L, \xi_V))$: double clamped case in vertical direction.

Substituting (C.4) and (C.7) in (C.3), the restrained level RL_i can be expressed as a function of the rotational stiffness, $K_{r,i}$:

$$\begin{aligned}\mathrm{RL}_i &= \frac{K_{r,i}\cdot\Theta_i(\mathrm{RL}_i)}{M_i(\mathrm{RL}_i\to 1)}\\ &= K_{r,i}\frac{\Theta_i(\mathrm{RL}_i)\cdot 2EI_i}{2EI_i+K_{r,i}\cdot L}\cdot\frac{1}{M_i\cdot(\mathrm{RL}_i\to 1)}.\end{aligned}\tag{C.8}$$

Solving (C.8) by the rotational stiffness $K_{r,i}$, the following relation as a function of the restrained level RL_i can be found:

$$\begin{aligned}K_{r,i} &= 2\cdot\frac{EI_i}{L}\cdot\mathrm{RL}_i\\ &\cdot\frac{1}{((\Theta_i(\mathrm{RL}_i=0)\cdot 2EI_i)/(M_i(\mathrm{RL}_i\to 1)\cdot L)-\mathrm{RL}_i)}.\end{aligned}\tag{C.9}$$

For a symmetric load applied on a symmetric constrained beam, it can be simply demonstrated that

$$M_i(\mathrm{RL}_i\longrightarrow 1)=\frac{\Theta_i(\mathrm{RL}_i=0)\cdot 2EI_i}{L}.\tag{C.10}$$

Using the previous equation in (C.9), the rotational stiffness as a function of RL_i can be expressed and simplified as

$$K_{r,i}=2\cdot\frac{EI_i}{L}\cdot\frac{\mathrm{RL}_i}{(1-\mathrm{RL}_i)}.\tag{C.11}$$

That is the demonstration of (14).

C.2. Derivation of (16). Let us define a nondimensional Rotation-to-Deflection ratio, (RD_i):

$$\mathrm{RD}_i=\frac{\Theta_i(\mathrm{RL}_i)\cdot L}{\delta_i(\mathrm{RL}_i)},\tag{C.12}$$

where $\Theta_i(\mathrm{RL}_i)$ and $\delta_i(\mathrm{RL}_i)$ are the end rotation and the midspan deflection due to a uniform load. The last deflection term can be expressed as sum of simply supported midspan beam deflection $\delta_i(\mathrm{RL}_i=0)$ and midspan deflection due to the end moments $M_i(\mathrm{RL}_i\to 1)$ as follows:

$$\delta_i(\mathrm{RL}_i)=\delta_i(\mathrm{RL}_i=0)-\frac{M_i(\mathrm{RL}_i)\cdot L^2}{8EI_i}.\tag{C.13}$$

Substituting (C.7), (C.11), and (C.13) in (C.12), the nondimensional Rotation-to-Deflection ratio can be expressed as

$$\begin{aligned}\mathrm{RD}_i &= \Theta_i(\mathrm{RL}_i=0)\cdot(1-\mathrm{RL}_i)\\ &\cdot\frac{L}{\delta_i(\mathrm{RL}_i=0)-(\mathrm{RL}_i\cdot M_i(\mathrm{RL}_i\to 1)\cdot L^2)/8EI_i}.\end{aligned}\tag{C.14}$$

Solving (C.14) by the restrained level, RL_i, the following relation as a function of the Rotation-to-Deflection ratio RD_i can be derived:

$$\begin{aligned}&\mathrm{RL}_i\\ &=\frac{(1-(\mathrm{RD}_i\cdot\delta_i(\mathrm{RL}_i=0))/(\Theta_i(\mathrm{RL}_i=0)\cdot L))}{(1-(\mathrm{RD}_i\cdot M_i(\mathrm{RL}_i\to 1)\cdot L)/(\Theta_i(\mathrm{RL}_i=0)\cdot 8EI_i))}.\end{aligned}\tag{C.15}$$

Finally, substituting the expression of $\delta_i(\mathrm{RL}_i=0)$, $\Theta_i(\mathrm{RL}_i=0)$, and $M_i(\mathrm{RL}_i\to 1)$ due to a uniform load pattern, the parameter RD_i can be expressed more simply as

$$\mathrm{RL}_i=\frac{4-1.25\cdot\mathrm{RD}_i}{4-\mathrm{RD}_i}.\tag{C.16}$$

That is the demonstration of (16).

C.3. Derivation of (22). The peak modal acceleration, $\widehat{\ddot{\eta}}_i(\mathrm{RL}_i,\alpha_i,L,\xi_i)$, is expressed in terms of a TFRF $(\mathrm{RL}_i,\alpha_i,L,\xi_i)$:

$$\begin{aligned}\widehat{\ddot{\eta}}_i(\mathrm{RL}_i,\alpha_i,L,\xi_i) &= \frac{\overline{\mathrm{DLF}_i}\cdot\overline{W}}{2\xi_i}\cdot\frac{1}{m_i}\\ &\cdot\varphi_i(\mathrm{RL}_i,\alpha_i,L,\xi_i).\end{aligned}\tag{C.17}$$

Since change of support conditions influences mode shapes and thus acceleration response, a boundary factor, $\mathrm{BF}_i(\mathrm{RL}_i,\alpha_i,L,\xi_i)$, is defined as

$$\mathrm{BF}_i(\mathrm{RL}_i,\alpha_i,L,\xi_i)=\frac{\widehat{\ddot{\eta}}_i(\mathrm{RL}_i,\alpha_i,L,\xi_i)}{\widehat{\ddot{\eta}}_i(\mathrm{RL}_i=0,\alpha_i,L,\xi_i)}.\tag{C.18}$$

The boundary factor is the ratio between the peak modal acceleration evaluated for arbitrary boundary conditions, $\widehat{\ddot{\eta}}_i(\mathrm{RL}_i,\alpha_i,L,\xi_i)$, and that evaluated for simply supported conditions, $\widehat{\ddot{\eta}}_i(\mathrm{RL}_i=0,\alpha_i,L,\xi_i)$. Substituting (C.17) in (C.18), the following can be obtained:

$$\begin{aligned}&\mathrm{BF}_i(\mathrm{RL}_i,\alpha_i,L,\xi_i)\\ &=\frac{(\overline{\mathrm{DLF}_i}\cdot\overline{W})/2\xi_i\cdot 1/m_i(\mathrm{RL}_i)\cdot\varphi_i(\mathrm{RL}_i,\alpha_i,L,\xi_i)}{(\overline{\mathrm{DLF}_i}\cdot\overline{W})/2\xi_i\cdot 1/m_i(\mathrm{RL}_i=0)\cdot\varphi_i(\mathrm{RL}_i=0,\alpha_i,L,\xi_i)}.\end{aligned}\tag{C.19}$$

Rearranging the previous equation,

$$\begin{aligned}&\mathrm{BF}_i(\mathrm{RL}_i,\alpha_i,L,\xi_i)\\ &=\frac{\cancel{(\overline{\mathrm{DLF}_i}\cdot\overline{W})/2\xi_i}}{\cancel{(\overline{\mathrm{DLF}_i}\cdot\overline{W})/2\xi_i}}\\ &\cdot\frac{1/m_i(\mathrm{RL}_i)}{1/m_i(\mathrm{RL}_i=0)}\frac{\varphi_i(\mathrm{RL}_i,\alpha_i,L,\xi_i)}{\varphi_i(\mathrm{RL}_i=0,\alpha_i,L,\xi_i)}\\ &=\underbrace{\frac{m_i(\mathrm{RL}_i=0)}{m_i(\mathrm{RL}_i)}}_{\mathrm{BF}_{m,i}(\mathrm{RL}_i)}\cdot\underbrace{\frac{\varphi_i(\mathrm{RL}_i,\alpha_i,L,\xi_i)}{\varphi_i(\mathrm{RL}_i=0,\alpha_i,L,\xi_i)}}_{\mathrm{BF}_{\varphi,i}(\mathrm{RL}_i,\alpha_i,L,\xi_i)}\end{aligned}\tag{C.20}$$

obtaining

$$\begin{aligned}\mathrm{BF}_i(\mathrm{RL}_i,\alpha_i,L,\xi_i) &= \mathrm{BF}_{m,i}(\mathrm{RL}_i)\\ &\cdot\mathrm{BF}_{\varphi,i}(\mathrm{RL}_i,\alpha_i,L,\xi_i)\\ &=\frac{m_i(\mathrm{RL}_i=0)}{m_i(\mathrm{RL}_i)}\\ &\cdot\frac{\varphi_i(\mathrm{RL}_i,\alpha_i,L,\xi_i)}{\varphi_i(\mathrm{RL}_i=0,\alpha_i,L,\xi_i)}.\end{aligned}\tag{C.21}$$

That is the demonstration of (22).

Conflicts of Interest

The authors declare that they have no conflicts of interest.

Acknowledgments

The authors express their personal thanks and appreciation to the Consorzio Interuniversitario di Ricerca Me.S.E. for having funded the publication and dissemination of these research results.

References

[1] H. Petroski, *To Engineer Is Human: The Role of Failure in Successful Design*, Vintage books New York, New York, NY, USA, 1992.

[2] B. Wolmuth and J. Surtees, "Crowd-related failure of bridges," *Proceedings of the Institution of Civil Engineers: Civil Engineering*, vol. 156, no. 3, pp. 116–123, 2003.

[3] C. Tilden, "Kinetic effects of crowds," *Transactions of the American Society of Civil Engineers*, vol. 76, no. 1, pp. 2107–2126, 1913.

[4] Á. Cunha and C. Moutinho, "Active control of vibrations in pedestrian bridges," in *Proceedings of the Conference of the European Association for Structural Dynamics (Eurodyn '99)*, 1999.

[5] F. Ricciardelli and C. Demartino, "Design of footbridges against pedestrian-induced vibrations," *Journal of Bridge Engineering*, Article ID C4015003, pp. 1–13, 2016.

[6] K. Van Nimmen, G. Lombaert, G. De Roeck, and P. Van den Broeck, "Vibration serviceability of footbridges: evaluation of the current codes of practice," *Engineering Structures*, vol. 59, pp. 448–461, 2014.

[7] J. Wheeler, "Prediction and control of pedestrian-induced vibration in footbridges," *Journal of the Structural Division*, vol. 108, no. 9, pp. 2045–2065, 1982.

[8] S. Živanović, A. Pavic, and P. Reynolds, "Vibration serviceability of footbridges under human-induced excitation: a literature review," *Journal of Sound and Vibration*, vol. 279, no. 1-2, pp. 1–74, 2005.

[9] E. T. Ingólfsson, C. T. Georgakis, and J. Jönsson, "Pedestrian-induced lateral vibrations of footbridges: a literature review," *Engineering Structures*, vol. 45, pp. 21–52, 2012.

[10] L. Pedersen and C. Frier, "Sensitivity of footbridge vibrations to stochastic walking parameters," *Journal of Sound and Vibration*, vol. 329, no. 13, pp. 2683–2701, 2010.

[11] A. Avossa, R. Di Camillo, and P. Malangone, "Performance-based retrofit of a prestressed concrete road bridge in seismic area, Life-Cycle and Sustainability of Civil Infrastructure Systems," in *Proceedings of the 3rd International Symposium on Life-Cycle Civil Engineering (IALCCE '12)*, CRC Press, Vienna, Austria, 2012.

[12] A. M. Avossa and P. Malangone, "Seismic retrofit of a prestressed concrete road bridge," *Ingegneria Sismica (International Journal of Earthquake Engineering)*, vol. 29, no. 4, pp. 5–25, 2012.

[13] C. Demartino and F. Ricciardelli, "Aerodynamic stability of ice-accreted bridge cables," *Journal of Fluids and Structures*, vol. 52, pp. 81–100, 2015.

[14] C. Demartino, H. H. Koss, C. T. Georgakis, and F. Ricciardelli, "Effects of ice accretion on the aerodynamics of bridge cables," *Journal of Wind Engineering & Industrial Aerodynamics*, vol. 138, pp. 98–119, 2015.

[15] C. Demartino, J. Wu, and Y. Xiao, "Experimental and numerical study on the behavior of circular RC columns under impact loading," *Procedia Engineering*, vol. 199, pp. 2457–2462, 2017.

[16] C. Demartino, J. Wu, and Y. Xiao, "Response of shear-deficient reinforced circular RC columns under lateral impact loading," *International Journal of Impact Engineering*, vol. 109, pp. 196–213, 2017.

[17] J. M. W. Brownjohn, A. Pavic, and P. A. Omenzetter, "A spectral density approach for modelling continuous vertical forces on pedestrian structures due to walking," *Canadian Journal of Civil Engineering*, vol. 31, no. 1, pp. 65–77, 2004.

[18] A. Pizzimenti and F. Ricciardelli, "Experimental evaluation of the dynamic lateral loading of footbridges by walking pedestrians," in *Proceedings of the EURODYN '05*, vol. 1, pp. 435–440, 2005.

[19] F. Ricciardelli and A. D. Pizzimenti, "Lateral walking-induced forces on footbridges," *Journal of Bridge Engineering*, vol. 12, no. 6, pp. 677–688, 2007.

[20] C. Butz, *Beitrag zur Berechnung fußgänger induzierte Brückenschwingungen [Ph.D. thesis]*, Shaker Verlag Aachen, Aachen, Germany, 2006.

[21] C. Heinemeyer, C. Butz, A. Keil et al., "Design of lightweight footbridges for human induced vibrations," in *Background Document in Support to The Implementation, Harmonization and Further Development of The Eurocodes*, 2009.

[22] S. Živanović, A. Pavić, and P. Reynolds, "Probability-based prediction of multi-mode vibration response to walking excitation," *Engineering Structures*, vol. 29, no. 6, pp. 942–954, 2007.

[23] E. Ingólfsson, C. Georgakis, and M. Svendsen, "Vertical footbridge vibrations: details regarding and experimental validation of the response spectrum methodology," in *Proceedings of the 3rd international conference on footbridge*, 2008.

[24] G. Piccardo and F. Tubino, "Simplified procedures for vibration serviceability analysis of footbridges subjected to realistic walking loads," *Computers & Structures*, vol. 87, no. 13-14, pp. 890–903, 2009.

[25] S. Živanović, A. Pavić, and E. T. Ingólfsson, "Modeling spatially unrestricted pedestrian traffic on footbridges," *Journal of Structural Engineering*, vol. 136, no. 10, pp. 1296–1308, 2010.

[26] CEN, Eurocode 5: Design of timber structures, Comité Européen de Normalisation, 2005.

[27] ISO, Bases for design of structures-Serviceability of buildigns and walkways against vibration, 2007.

[28] Sétra, Technical guide-Footbridges: Assessment of vibrational behaviour of footbridges under pedestrian loading, 2006.

[29] BSI, U.K. national annex to Eurocode 1, 2008.

[30] J. Brownjohn, P. Fok, M. Roche, and P. Omenzetter, "Long span steel pedestrian bridge at Singapore Changi Airport—part 2: crowd loading tests and vibration mitigation measures," *The Structural Engineer*, vol. 82, no. 16, pp. 28–34, 2004.

[31] E. T. Ingólfsson and C. T. Georgakis, "A stochastic load model for pedestrian-induced lateral forces on footbridges," *Engineering Structures*, vol. 33, no. 12, pp. 3454–3470, 2011.

[32] G. Piccardo and F. Tubino, "Equivalent spectral model and maximum dynamic response for the serviceability analysis of footbridges," *Engineering Structures*, vol. 40, pp. 445–456, 2012.

[33] A. G. Davenport, "Note on the distribution of the largest value of a random function with application to gust loading," in *Proceedings of the ICE*, vol. 28, pp. 187–196, 1964.

[34] A. M. Avossa, C. Demartino, and F. Ricciardelli, "Design procedures for footbridges subjected to walking loads: comparison

and remarks," *The Baltic Journal of Road and Bridge Engineering*, vol. 12, no. 2, pp. 94–105, 2017.

[35] A. M. Avossa, C. Demartino, and F. Ricciardelli, "Probability distribution of footbridge peak acceleration to single and multiple crossing walkers," *Procedia Engineering*, vol. 199, pp. 2766–2771, 2017.

[36] CEN, Eurocode 0: Basis of structural design, Comité Européen de Normalisation, 2002.

[37] ISO, 2394 General Principles on Reliability for Structures, 1998.

[38] F. Beely, "Zur Mechanik des Stehens," *Longenbeck's Archiv Für Klinische Chirurgie*, vol. 27, pp. 457–471, 1882.

[39] H. Elftman, "A cinematic study of the distribution of pressure in the human foot," *The Anatomical Record*, vol. 59, no. 4, pp. 481–491, 1934.

[40] C. J. T. Van Uden and M. P. Besser, "Test-retest reliability of temporal and spatial gait characteristics measured with an instrumented walkway system (GAITRite)," *BMC Musculoskeletal Disorders*, vol. 5, no. 1, article 13, 2004.

[41] S. Zivanovic, A. Pavic, P. Reynolds, and P. Vujovic', "Dynamic analysis of lively footbridge under everyday pedestrian traffic," in *Proceedings of the 6th European Conference on Structural Dynamics*, vol. 1, pp. 453–459, 2005.

[42] N. A. Borghese, L. Bianchi, and F. Lacquaniti, "Kinematic deferminants of human locomotion," *The Journal of Physiology*, vol. 494, no. 3, pp. 863–879, 1996.

[43] L. Li, E. C. H. Van Den Bogert, G. E. Caldwell, R. E. A. Van Emmerik, and J. Hamill, "Coordination patterns of walking and running at similar speed and stride frequency," *Human Movement Science*, vol. 18, no. 1, pp. 67–85, 1999.

[44] J. L. Lelas, G. J. Merriman, P. O. Riley, and D. C. Kerrigan, "Predicting peak kinematic and kinetic parameters from gait speed," *Gait & Posture*, vol. 17, no. 2, pp. 106–112, 2003.

[45] F. Venuti and L. Bruno, "Crowd-structure interaction in lively footbridges under synchronous lateral excitation: a literature review," *Physics of Life Reviews*, vol. 6, no. 3, pp. 176–206, 2009.

[46] F. Ricciardelli, C. Briatico, E. Ingólfsson, and C. Georgakis, "Experimental validation and calibration of pedestrian loading models for footbridges," *Experimental Vibration Analysis for Civil Engineering Structures*, 2006.

[47] M. Y. Zarrugh, F. N. Todd, and H. J. Ralston, "Optimization of energy expenditure during level walking," *European Journal of Applied Physiology*, vol. 33, no. 4, pp. 293–306, 1974.

[48] A. Pachi and T. Ji, "Frequency and velocity of people walking," *The Structural Engineer*, vol. 83, no. 3, pp. 36–40, 2005.

[49] S. Zivanovic, V. Racic, I. El-Bahnasy, and A. Pavic, "Statistical characterisation of parameters defining human walking as observed on an indoor passerelle," in *Proceedings of the Experimental Vibration Analysis for Civil Engineering Structures, EVACES '07*, pp. 219–225, 2007.

[50] E. T. Ingólfsson, C. T. Georgakis, F. Ricciardelli, and J. Jönsson, "Experimental identification of pedestrian-induced lateral forces on footbridges," *Journal of Sound and Vibration*, vol. 330, no. 6, pp. 1265–1284, 2011.

[51] Y. Matsumoto, T. Nishioka, H. Shiojiri, and K. Matsuzaki, "Dynamic design of footbridges," in *Proceedings of the IABSE Proceeding*, 1978.

[52] C. Butz, M. Feldmann, C. Heinemeyer et al., "Advanced load models for synchronous pedestrian excitation and optimised design guidelines for steel foot bridges (SYNPEX)," *Endbericht und Zwischenberichte zum RFCS Projekt RFS-CR*, vol. 3, article 19, 2007.

[53] V. Racic, A. Pavic, and J. M. W. Brownjohn, "Experimental identification and analytical modelling of human walking forces: literature review," *Journal of Sound and Vibration*, vol. 326, no. 1-2, pp. 1–49, 2009.

[54] F. Ricciardelli, M. Mafrici, and E. T. Ingólfsson, "Lateral pedestrian-induced vibrations of footbridges: characteristics of walking forces," *Journal of Bridge Engineering*, vol. 19, no. 9, Article ID 04014035, 2014.

[55] J. H. Macdonald, "Lateral excitation of bridges by balancing pedestrians," *Proceedings of the Royal Society A Mathematical, Physical and Engineering Sciences*, 2008.

[56] Q. S. Yang, J. W. Qin, and S. S. Law, "A three-dimensional human walking model," *Journal of Sound and Vibration*, vol. 357, pp. 437–456, 2015.

[57] J. Blanchard, B. Davies, and J. Smith, "Design criteria and analysis for dynamic loading of footbridges," in *Proceedings of the Proceeding of a Symposium on Dynamic Behaviour of Bridges at the Transport and Road Research Laboratory*, 1977.

[58] H. Bachmann, A. Pretlove, and J. Rainer, Dynamic forces from rythmical human body motions,.

[59] Y. Kajikawa, "Some considerations on ergonomical serviceability analysis of pedestrian bridge vibrations," in *Proceedings of the JSCE*, vol. 325, pp. 23–33, 1982 (Japanese).

[60] M. Yoneda, "A simplified method to evaluate pedestrian-induced maximum response of cable-supported pedestrian bridges," in *Proceedings of the International Conference on the Design and Dynamic Behaviour of footbridges*, 2002.

[61] S. Kerr, *Human induced loading on staircases [Ph.D. thesis]*, University of London, London, UK, 1998.

[62] P. Young, "Improved floor vibration prediction methodologies," in *Proceedings of the ARUP vibration seminar*, vol. 4, 2001.

[63] H. Bachmann and W. Ammann, "Vibrations in structures: induced by man and machines," *Vibrations in structures: induced by man and machines*, vol. 3, 1987.

[64] M. Fareed and M. Afzal, "Evidence of inbreeding depression on height, weight, and body mass index: a population-based child cohort study," *American Journal of Human Biology*, vol. 26, no. 6, pp. 784–795, 2014.

[65] S. C. Walpole, D. Prieto-Merino, P. Edwards, J. Cleland, G. Stevens, and I. Roberts, "The weight of nations: an estimation of adult human biomass," *BMC Public Health*, vol. 12, no. 1, article 439, 2012.

[66] L. Bruno, F. Venuti, and V. Nascé, "Pedestrian-induced torsional vibrations of suspended footbridges: proposal and evaluation of vibration countermeasures," *Engineering Structures*, vol. 36, pp. 228–238, 2012.

[67] H. Bachmann, *Vibration Problems in Structures: Practical Guidelines*, Springer, Berlin, Germany, 1995.

[68] M. Ferraioli, A. M. Avossa, and F. Formato, "Base isolation seismic retrofit of a hospital building in Italy: design and construction," in *Proceedings of the Final Conference on COST Action C26: Urban Habitat Constructions under Catastrophic Events*, pp. 835–840, September 2010.

[69] A. M. Avossa and G. Pianese, "Damping effects on the seismic response of base-isolated structures with LRB devices," *Ingegneria Sismica*, vol. 34, no. 2, pp. 3–29, 2017.

[70] Y. Kubota and T. Kishimoto, "Structural continuity and relativity for footbridge design," in *Proceedings of the Footbridges 2008: Third International Conference*, 2008.

[71] CEN, Eurocode 1: Actions on structures, omité Européen de Normalisation, 2003.

[72] CEN, Eurocode 3: Design of Steel Structures, Comité Européen de Normalisation, 2005.

[73] FIB, Guidelines for the design of footbridges, Fédération Internationale du Béton, Lausanne, Switzerland, 2005.

[74] M. Abu-Hilal and M. Mohsen, "Vibration of beams with general boundary conditions due to a moving harmonic load," *Journal of Sound and Vibration*, vol. 232, no. 4, pp. 703–717, 2000.

[75] F. Ricciardelli and C. Briatico, "Transient response of supported beams to moving forces with sinusoidal time variation," *Journal of Engineering Mechanics*, vol. 137, no. 6, pp. 422–430, 2011.

[76] G. Piccardo and F. Tubino, "Dynamic response of Euler-Bernoulli beams to resonant harmonic moving loads," *Structural Engineering and Mechanics*, vol. 44, no. 5, pp. 681–704, 2012.

[77] A. Palmeri, F. Ricciardelli, G. Muscolino, and A. De Luca, "Random vibration of systems with viscoelastic memory," *Journal of Engineering Mechanics*, vol. 130, no. 9, pp. 1052–1061, 2004.

[78] H. Karadeniz and T. Vrouwenvelder, Overview reliability methods, vol. 5, 2003.

[79] M. Griffin, Handbook of human vibration, 1990.

[80] N. Mansfield, *Human Response to Vibration*, CRC Press, Boca Raton, Fla, USA, 2004.

[81] ISO, ISO 2631: Mechanical vibration and shock-Evaluation of human exposure to whole-body vibration-Part 1: General requirements, 1997.

[82] MIT, *Ministerial Decree: NTC 2008-Norme tecniche per le costruzioni*, Ministero delle Infrastrutture, italy, 2008.

[83] S. CSI, Ver. 14.00, integrated finite element analysis and design of structures basic analysis reference manual, 2010.